UHASSELT
KNOWLEDGE IN ACTION

Maastricht University

Faculty of Medicine and Life Sciences
School for Life Sciences
Master of Biomedical Sciences

Master's thesis

PDE4D inhibition to improve peripheral myelination, Schwann cell differentiation and motor function in Charcot-Marie-Tooth disease type 1A

Darren Jacobs

Thesis presented in fulfillment of the requirements for the degree of Master of Biomedical Sciences, specialization Molecular Mechanisms in Health and Disease

SUPERVISOR :

dr. Elisabeth PICCART

MENTOR :

Mevrouw Melissa SCHEPERS

2020
2021

Transnational University Limburg is a unique collaboration of two universities in two countries: the University of Hasselt and Maastricht University.

UHASSELT
KNOWLEDGE IN ACTION

www.uhasselt.be
Universiteit Hasselt
Campus Hasselt:
Martelarenlaan 42 | 3500 Hasselt
Campus Diepenbeek:
Agoralaan Gebouw D | 3590 Diepenbeek

UHASSELT
KNOWLEDGE IN ACTION

Maastricht University

Faculty of Medicine and Life Sciences
School for Life Sciences
Master of Biomedical Sciences

Master's thesis

PDE4D inhibition to improve peripheral myelination, Schwann cell differentiation and motor function in Charcot-Marie-Tooth disease type 1A

Darren Jacobs

Thesis presented in fulfillment of the requirements for the degree of Master of Biomedical Sciences, specialization Molecular Mechanisms in Health and Disease

SUPERVISOR :

dr. Elisabeth PICCART

MENTOR :

Mevrouw Melissa SCHEPERS

PDE4D inhibition to improve peripheral myelination, Schwann cell differentiation and motor function in Charcot-Marie-Tooth disease type 1A

Darren Jacobs[1], Tim Vangansewinkel[1,3], Melissa Schepers[3], Karen Libberecht[1,3], Elisabeth Piccart[3], Esther Wolfs[1] and Tim Vanmierlo[3]

[1]Cardio and Organ Systems research group, Biomedical Research Institute, Universiteit Hasselt, Campus Diepenbeek, Agoralaan Gebouw C - B-3590 Diepenbeek
[2]Neuroimmunology research group, Biomedical Research Institute, Universiteit Hasselt, Campus Diepenbeek, Agoralaan Gebouw C - B-3590 Diepenbeek
[3]VIB, Center for Brain & Disease Research, Laboratory of Neurobiology, Leuven, Belgium

*Running title: *PDE4D inhibition for functional repair in CMT1A*

To whom correspondence should be addressed:
Esther Wolfs, Tel: +3211269296; Email: esther.wolfs@uhasselt.be
Tim Vanmierlo, Tel: +3211269228; Email: tim.vanmierlo@uhasselt.be

Keywords: CMT1A, remyelination, differentiation, Schwann cell, PDE4D, motor function

ABSTRACT

Charcot-Marie-Tooth disease type 1A (CMT1A) is an inherited neuropathy of the peripheral nervous system. Symptoms include distal muscle weakness and atrophy, as well as sensory loss. Currently, no therapies for CMT1A are available. CMT1A is characterized by Schwann cell (SC) dedifferentiation and demyelination. The differentiation of SCs to the myelinating phenotype and the subsequent myelination process are positively regulated by cAMP. Therefore, we hypothesized that elevating intracellular cAMP levels by inhibiting PDE4D, a main cAMP-hydrolyzing enzyme in SCs, can stimulate SC differentiation, myelination and subsequent functional repair in the C3-PMP22 mouse model. Primary SCs were treated with 3 different inhibitors (GEBR-32a, BPN14770 and Roflumilast) and their differentiation to the myelinating phenotype was investigated by assessing gene expression of several SC differentiation markers by qPCR, as well as the protein levels of several markers using immunocytochemistry. These experiments were inconclusive due to a sample size of 1 and need to be repeated. Secondly, the therapeutic potential of PDE4D inhibitor GEBR-32a was evaluated *in vivo*. Mice were injected with 0.3 mg/kg GEBR-32a twice per day for 7 weeks, and motor function was assessed using several behavioral assays before treatment as well as during treatment. Here, we found that GEBR-32a treatment significantly improves endurance, balance and coordination in C3-PMP22 mice. Furthermore, electrophysiological recordings showed a significant increase in nerve conduction speed, indicating a boost in myelination. In conclusion, these findings indicate a very promising therapeutic potential of PDE4D inhibition in CMT1A, although the exact molecular mechanisms need to be evaluated *in vitro*.

INTRODUCTION

Charcot-Marie-Tooth disease (CMT) is the most common inherited neuropathy of the peripheral nervous system (PNS), affecting about 1 in 2500 individuals globally (1). There are several subclasses of the disease, based on electrophysiological aberrations (axonal, demyelinating, intermediate) and different patterns of inheritance (autosomal dominant, autosomal recessive, X-linked) (2). The most common group of CMT cases are the autosomal dominant demyelinating type or type 1. Other types include autosomal dominant axonal (CMT2), autosomal recessive (CMT4), and X-linked intermediate (CMTX) (3). Approximately 60% of all genetically confirmed CMT cases are caused by an autosomal dominant duplication of the *PMP22* gene, resulting in demyelinating neuropathy. This class is termed CMT type 1A (CMT1A) (3). Clinical symptoms of

CMT1A mainly start in the first two decades of life. These include muscle weakness and atrophy, as well as sensory loss. Overall, the legs are more frequently and more severely affected than the upper body. Hand and arm weakness can occur but lags behind the development of leg and foot weakness. The hallmark features of CMT1A are foot deformities due to distal muscle weakness, more specifically pes cavus (high arches) and hammertoes. Generally, 1 – 7 % of patients become wheelchair dependent (2, 4). Currently, there is no effective therapy for CMT1A (2).

On the cellular level, CMT1A is characterized by demyelination, meaning loss or disruption of the myelin sheath. In the peripheral nerve, the myelin sheath is produced by Schwann cells (SCs) by wrapping of their cell membrane around the axon in a tightly regulated manner. This lipid-rich structure acts as an electrical insulator. Two adjacent segments of myelin are separated by nodes of Ranvier. In this region, the axon is not covered by myelin. In an unmyelinated axon, an electrical impulse is propagated by local circuits of ion flow between the axonal membrane and extracellular space, which depolarize the adjacent regions of membrane in a continuous, sequential fashion. In contrast, in a myelinated axon, the axonal membrane is only exposed to the extracellular space at the nodes of Ranvier. Due to the high resistance of the myelin sheath, the generated circuit cannot flow through it, and therefore flows to and depolarizes the membrane at the next node. Due to the low capacitance of the myelin sheath, little energy is required to depolarize the membrane between nodes, which together with the "jumping" of the excitation of the membrane results in much more rapid impulse conduction (5). Hence, failure of myelin production and maintenance results in impairment of electrical conduction, leading to clinical symptoms mostly consisting of loss of motor function and sensation, as is seen in diseases such as multiple sclerosis, leukodystrophies, and CMT (6).

Furthermore, the other significant process observed in CMT1A is SC dedifferentiation. SCs are one of the few examples of somatic cells retaining dedifferentiation capacity, meaning they can revert to an immature, proliferative, non-myelinating state (7). In general, this happens mainly in response to acute nerve injury, where SCs lose their myelinating phenotype in order to proliferate and secrete factors that protect the axon against further damage and promote axon regeneration (7, 8). However, the dedifferentiation to these "repair cells" also occurs in chronic demyelinating disorders, including CMT. It is hypothesized that this is a defense mechanism to protect the neuron against secondary damage in chronic neuropathies, but the exact cause and mechanisms remain elusive (8).

On the molecular level, CMT1A is caused by a heterozygous 1.4 MB duplication of chromosome segment 17p11.2, containing the *PMP22* gene. This duplication leads to overexpression of *PMP22*, which was found to be the sole driver of demyelinating neuropathy. However, the exact mechanisms behind *PMP22* overexpression causing neuropathy remain unknown (2, 4). PMP22 is an integral membrane protein of peripheral myelin, playing an essential role in SC physiology. A particularly important function of PMP22 is the protection of nerve fibers against mechanical compression, which can interrupt impulse conduction (9). This function of PMP22 becomes apparent in hereditary neuropathy with liability to pressure palsies (HNPP), where one copy of *PMP22* is deleted. This disorder is characterized by conduction block due to nerve compression. However, the overall physiological roles of PMP22 remain largely unknown (10).

In the context of CMT1A, overexpression of *PMP22* disrupts a wide range of physiological processes in SCs. Overexpression of *PMP22* was shown to reduce cholesterol and lipid biosynthesis, which has a substantial effect on myelination (11, 12). Moreover, *PMP22* overexpression increases Ca^{2+} influx in SCs by augmenting the expression of the purinoceptor P2X7. This increased influx was shown to have a pathogenic connection to aberrant myelination (13). Another hypothesis is that *PMP22* overexpression increases the number of misfolded proteins, and this may overwhelm the protein degradation system (14). It is likely an accumulation of effects that ultimately results in loss of the myelinating capacity of SCs.

Proliferating SC precursors require axonal signals to exit the cell cycle and differentiate to the myelinating phenotype *in vivo*. Neuregulin (NRG) in particular, an axonal membrane protein, plays a critical role in this process by activating the MEK/ERK and AKT pathways in SCs, ultimately stimulating myelination (6, 15). The second

messenger molecule cyclic adenosine monophosphate (cAMP) enhances the effect of NRG by synergistically increasing the activation of MEK/ERK and AKT (16). Additionally, the onset and progression of myelination are directly dependent on the balance between positive and negative transcriptional regulators. The master positive regulator of myelination is Krox-20/Egr-2. On the other hand, the main negative regulator is c-Jun, which inhibits myelination and stimulates dedifferentiation (17). cAMP activates the Protein Kinase A (PKA) and Exchange Protein Activated by cAMP (EPAC) pathways and was observed to directly increase the Krox-20 to c-Jun ratio in SC *in vitro* (15). Thus, in combination with extracellular signals, cAMP is a potent stimulator of SC differentiation and is required for the myelination program (15, 18-20).

cAMP signaling is regulated positively by adenylyl cyclase (AC) and negatively by phosphodiesterases (PDEs). So far, the G-protein-coupled receptor 126 (GPR126), which is activated by various ECM proteins, is the only known receptor to drive SC differentiation through AC activation and subsequent cAMP elevation (21). On the other hand, PDEs are a family of hydrolases that control the intracellular levels of cAMP and cGMP by degrading them. They are the only known terminators of cyclic nucleotide signals (22). PDE4, a subfamily of PDEs, is the most important PDE selectively hydrolyzing cAMP. It is highly expressed in immune and neural cells, including glia. PDE4 inhibitors have been widely investigated as therapeutic compounds to treat inflammatory diseases (22). Recently, progress has been made in using PDE4 inhibitors to promote remyelination in multiple sclerosis (MS). Treatment of rats with the PDE4 inhibitor Rolipram resulted in enhanced remyelination after ethidium bromide-induced demyelination (23). However, Rolipram was shown to induce unwanted side effects including emesis, hindering clinical use (24, 25). Therefore, development of isoform-specific inhibitors commenced (24). PDE4 consists of 4 isoforms: PDE4A, -B, -C and -D, from which PDE4D is prominent in SCs (26). Over the past years, PDE4D has emerged as a viable target for drug development against cognitive deficits, where cAMP also plays a pivotal role (25). Selective PDE4D inhibitors showed a higher therapeutic index than general PDE4 inhibitors such as Rolipram, generating the desired effects at doses devoid of unwanted side effects (27). Recently, a novel PDE4D selective inhibitor was developed, named GEBR-32a. This compound showed great therapeutic potential in the context of cognition enhancement by possessing a favorable toxicological and pharmacokinetic profile and potently increasing intracellular cAMP levels (24).

In this study, we investigated whether PDE4D inhibition by GEBR-32a can induce SC differentiation and remyelination in CMT1A. We hypothesized that inhibition of PDE4D enhances remyelination and promotes SC redifferentiation in primary CMT1A SCs *in vitro*, in conjunction with improving motor function in a CMT1A mouse model. Here, the C3-PMP22 mouse model was used, which expresses 3 to 4 copies of the human *PMP22* gene and shows the same symptoms as human patients (28).

EXPERIMENTAL PROCEDURES

Primary Schwann cell isolation, cryopreservation and cell culture – Schwann cells were isolated from 6 week-old and 1-year-old wild type (WT) and C3-PMP22 mice as described in Andersen et al. 2018 (29). Both sciatic nerves and brachial plexuses were isolated for Schwann cell harvest. Briefly, after enzymatic digestion with collagenase I and dispase II (Millipore, Burlington, USA), cell suspensions were drop plated in a petri dish. After a stable culture was established, cells were sorted using Fluorescence-Activated Cell Sorting (FACS), based on p75 positivity to separate Schwann cells (p75+) from fibroblasts (p75-) (Suppl. Fig. 1). The primary antibody used was Rabbit anti-p75 (Cell Signaling Technologies, Danvers, USA). Cells were kept in culture in DMEM (D6429, Sigma Life Science, Saint Louis, USA) supplemented with 10 % Fetal Bovine Serum, 1% penicillin/streptomycin, 10 mM Forskolin, 200µg/ml Neuregulin and 50µg/ml PDGF. Cells were regularly passaged.

In vitro PDE4 inhibitor treatment – Primary Schwann cells were treated with either 1 µM GEBR-32a, 1µM BPN14770, 1µM Roflumilast or vehicle control (DMSO). Treatment started one day after seeding with a full medium change to DMEM containing the appropriate treatment. Two more 50% medium change were performed every 2 days, with sample collection on day 7.

RNA isolation and Quantitative PCR – Schwann cells were seeded in a 24-well plate at an initial density of $25*10^3$ cells/well. After the treatment period, cells were lysed using Qiazol® Lysis Reagent (Qiagen, Netherlands). Lysates were stored at -80°C until further use. Total RNA was extracted by phase separation using chloroform, followed by precipitating total RNA from the water phase using glycogen and 2-isopropanol. Finally, RNA was washed several times using 75% ethanol and suspended in RNA-free water. RNA purity and concentration were determined using a NanoDrop® spectrophotometer (Isogen Life Science, Utrecht, Netherlands). Lastly, RNA was reverse transcribed to cDNA at a final concentration of 5 ng/µl by PCR using the Qscript™ cDNA synthesis kit (Quanta Biosciences, Gaithersburg, USA) according to the manufacturer's protocol and stored at -20°C until further use. qPCR was conducted using Fast SYBR™ Green Master Mix on the StepOnePlus instrument (Applied Biosystems, Foster City, USA). Relative quantification of gene expression was performed using the comparative Ct method. Data were normalized to the most stable reference genes. The used primers are listed in Supplementary Table 1. All primers were purchased from Integrated DNA Technologies (Leuven, Belgium).

Immunocytochemistry – Cells were seeded on glass coverslips at an initial density of $10*10^3$ cells/coverslip. After the treatment period, cells were washed with PBS and fixed using 4% paraformaldehyde in PBS for 15 min. Cells were kept on PBS at 4°C until further use. Samples were permeabilized using 0,1% Triton X-100 for 15 min and blocked using Dako Protein Block (Dako, Carpinteria, USA) for 45 min, followed by primary antibody incubation (1:400 dilution) for 2h at room temperature or overnight at 4°C. The primary antibodies used are listed as the following: Rat anti-MPB (Merck Millipore, Germany), Rabbit anti-MPZ, Rabbit anti-c-Jun, Rabbit anti-Krox-20, Mouse anti-GFAP and Rabbit anti-SOX2 (Abcam, Cambridge, UK). After washing with PBS, secondary antibody incubation was performed for 1h (1:400 dilution). The secondary antibodies used are listed as the following: Alexa Fluor 488 donkey anti-Mouse, Alexa Fluor 555 donkey anti-rabbit, Alexa Fluor 488 Goat-anti-Rat and Alexa Fluor 555 Donkey anti-Mouse (Invitrogen, Carlsbad, USA). Nucleus staining was performed using 4′,6-diamidino-2-phenylindole (DAPI) for 10 min. All samples were visualized using a Leica DM4000 B LED automated upright microscope with Leica LAS X Life Science microscope software. The Leica DFC 450 C CCD camera was used for imaging (Leica, Wetzlar, Germany). Images were analyzed using ImageJ software.

Animals and in vivo study setup – All animal procedures were performed in accordance with institutional guidelines and approved by the ethical committee for animal experiments of Hasselt University. C3-PMP22 mice were kindly provided by Prof. Dr. Frank Baas (Amsterdam University) (30) and crossed with C57Bl6/J mice (The Jackson Laboratory, Bar Harbor, USA) to generate C3-PMP22 and WT littermates. Animals were housed in a temperature- and humidity-controlled conventional animal facility at Hasselt University in a 12h light/12h dark cycle, with ad libitum access to food and water. Two separate experiments were conducted in parallel. In the first cohort, male and female 15 – 20 week-old mice were divided into 3 groups (WT control n = 5; C3-PMP22 vehicle n = 4; C3-PMP22 treated n = 4). In the second cohort, male 30 – 35 week-old mice were divided into 3 groups (WT control n = 7; C3-PMP22 vehicle n = 5; C3-PMP22 treated n = 5). Both cohorts followed the same protocol. Mice were injected subcutaneously twice a day (with a 10h time window between both injections) with either DMSO (vehicle control) or 0.3 mg/kg GEBR-32a for 7 weeks. Baseline behavioral experiments were performed before commencing treatment and were repeated during week 3 of the treatment. Electrophysiological measurements were recorded during week 3 and week 6 of treatment. All behavioral experiments were scored blind.

Mouse genotyping – Genotyping of C3-PMP22 and WT mice was performed using conventional polymerase chain reaction (PCR) after DNA extraction from ear biopsies using the KAPA Express Extract kit (KAPA Biosystems, Wilmington, USA) according to the manufacturer's protocol. Primers used for amplification of the human PMP22 transgene are listed as the following: forward: 5'-TGGTGATGATGAGAAACAGT-3' and reverse: 5'-TGATTCTCTCTAGCAATCGA-3'. Primers were purchased from Integrated DNA Technologies (Leuven, Belgium).

Beam walking – beams of 18, 12 and 7 mm wide, 1m long and 3 cm high were used. The beams were suspended ~1m above the ground with a black end goal box (Suppl. Fig. 2). Mice were allowed to traverse the beam and the time taken to traverse the inner 80cm of the beam was measured. For each mouse, 3 successful runs were recorded. A successful run was defined as one continuous movement (no stopping/turning around).

Grid walking – The grid walkway was 1 m long, 10 cm wide and 10 cm high, with a grid size of 2x2 cm. The walkway was suspended ~1m above ground with a black end goal box. A camera was mounted underneath, filming the inner 80 cm of the walkway. Each mouse traversed the walkway 3 times. Videos were later analyzed to determine the number of foot slips made. Foot slips were defined as the animal attempting to place a hind paw and completely passing through the plane of the wire grid (Suppl. Fig 3). The average number of foot slips was calculated for each mouse.

Rotarod – An accelerating mouse-sized Rotarod (Ugo Basile, Italy) was used. 4 trials were performed using 4 – 40 RPM acceleration over the course of 5 min, with a minimum of 5 min rest between trials.

Grip strength – A wire grid was attached to a LabQuest® Newton meter (Vernier, USA). Mice were placed on the grid and pulled backwards by the tail. The maximum force before losing grip was recorded. For each mouse, 3 measurements were recorded with at least 5 min of rest between trials.

Hanging wire test – Mice were placed on a cage lid and turned upside down ~10cm above the cage. The latency to fall was recorded with a cutoff time of 2 min. For each mouse, 3 measurements were recorded with at least 5 min of rest between trials.

Pellet retrieval task – The training protocol was modified from Chen et al. 2014 (31). Briefly, mice were shaped by placing them inside the training chamber individually on day 1. After the first day, mice were food-restricted. They gained access to food for 2h per day for the remainder of the training period. On day 2, mice were placed inside the training chamber with ~10 pellets for their consumption. From day 3 onwards, forelimb dominance was determined as previously described (31). After forelimb dominance was determined for each animal, animals were scored on the final day as previously described (31). 30 attempts or 20 min (whichever came first) were recorded and scored (1, success; 2, dropped; 3, fail) (Suppl. Fig. 4). From these data, the success rate was calculated per animal. After initial training, no re-training was needed. After treatment, mice were immediately scored in the same way as the final day of training.

Electrophysiological measurements – Compound Muscle Action Potentials (CMAP) of the sciatic nerve were recorded in the animals using a NIM-Eclipse® System (Medtronic, Dublin, Ireland), following the protocol described by Pollari et al. (32). During week 3, stimulation was performed at 2,5 mA and 8 mA for WT and C3-PMP22 mice, respectively. During week 6, supramaximal stimulation was performed.

Statistical analysis – All statistical analyses were performed using Graphpad Prism 9.0.1 software (Graphpad Software, San Diego, USA). Groups were checked for normality using a Shapiro-Wilk test. When groups were normally distributed, they were compared using an unpaired t-test. When groups were not normally distributed, they were compared using the non-parametrical Mann-Whitney test. To compare three or more groups, a one-way ANOVA or non-parametric Kruskal-Wallis test was used. The significance level was set at 0.05. Data are presented as mean ± standard error of the mean (SEM).

RESULTS

PDE4D and -B isoform expression in wild type and C3-PMP22 Schwann cells – To confirm whether *PDE4D* is expressed in Schwann cells, as well as another PDE4 isoform commonly used as a therapeutic target, *PDE4B*, primary Schwann cells were isolated from both WT and C3-PMP22 mice. Gene expression of several *PDE4D* and *-B* isoforms was assessed using qPCR (Fig. 1). Of the isoforms investigated, *PDE4D* isoform 8 and *PDE4B* isoform 5 were not detected. Interestingly, all *PDE4D* isoforms investigated showed a trend towards higher expression in the C3-PMP22 SCs, although this increase is not statistically significant. The 3 *PDE4B* isoforms detected showed a rather mixed expression between the two genotypes.

The effect of PDE4(D) inhibition on Schwann cell marker gene expression – To assess the effect of PDE4(D) inhibition on the SC differentiation state *in vitro*, primary SCs isolated from both C3-PMP22 and WT mice were treated using 3 different inhibitors. First, the inhibitor of interest,

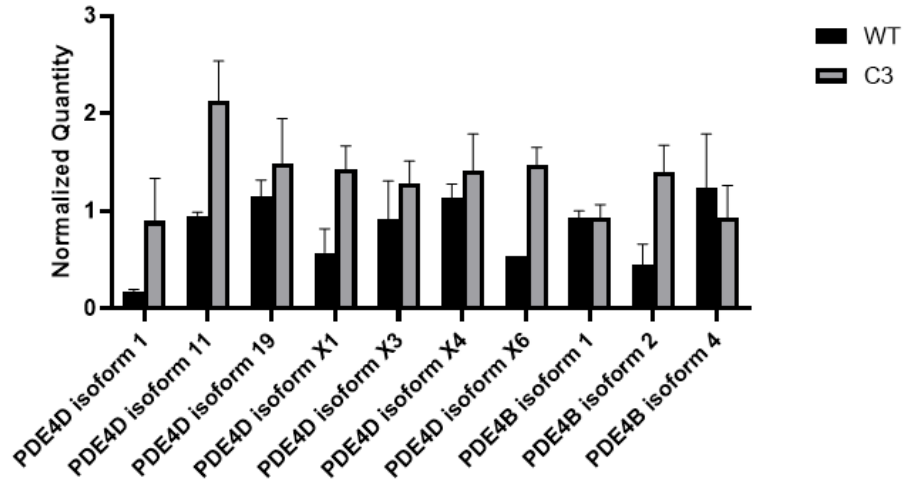

Fig. 1 – *PDE4D* and -*B* isoform expression in WT and C3-PMP22 Schwann cells. *PDE* expression was quantified using qPCR. The normalized quantities are shown. There are no significant differences between WT and C3-PMP22 Schwann cells. Not shown are PDE4D isoform 8 and PDE4B isoform 5, as no significant expression was detected. N = 3 for both genotypes. Statistical analysis: Mann-Whitney test. WT, wild type; C3, C3-PMP22.

GEBR-32a, along with another PDE4D-specific inhibitor, BPN14770 (BPN) were used. GEBR-32a binds to the catalytic domain of PDE4D, while BPN is an allosteric inhibitor of PDE4D. Lastly, the PDE4 pan-inhibitor Roflumilast was included for comparison. Cells were treated by incubating them with culture medium containing 1 µM of the appropriate compound for 6 days, with 50% medium changes every 2 days. After the treatment period, total RNA was extracted and qPCR was performed to investigate the expression of several markers (Fig. 2). It is important to note that all conditions have a sample size of 1, so no statistical analysis was performed. When looking at the 2 main regulators of myelination, *Krox-20* and *c-Jun*, GEBR-32a treatment increased *Krox-20* expression 3-fold in C3-PMP22 cells compared to vehicle (DMSO) treated C3-PMP22 cells (Fig 2A). However, in WT cells, while GEBR-32a also resulted in an increase, BPN had the highest impact on *Krox-20* expression while it did not affect *Krox-20* expression in C3-PMP22 cells. Roflumilast did not affect *Krox-20* expression in both genotypes. When examining *c-Jun*, surprisingly, inhibitor treatment appears to increase its expression in both genotypes, with Roflumilast exerting the most profound effect (Fig. 2B). When looking at myelin proteins MPZ and MBP, it is interesting to note that the C3-PMP22 cells showed a much higher *MBP* expression compared to the WT cells (50-fold), with Roflumilast increasing its expression in both genotypes, but the other 2 inhibitors having no large effect (Fig. 2C). On the other hand, *MPZ* expression does not appear to be influenced greatly by inhibitor treatment. Moreover, the C3-PMP22 cells also show higher *MPZ* expression, but not as drastically as *MBP* (Fig. 2D). Next, another transcription factor crucial for myelination, *Oct-6*, appears to increase in expression after treatment with all 3 inhibitors, with Roflumilast having the largest effect (Fig. 2E). On the other hand, *SOX2*, a negative regulator of differentiation to the myelinating phenotype, appears to decrease slightly after GEBR-32a treatment in C3-PMP22 and WT cells, but the effect of the other inhibitors is smaller (Fig. 2F). Next, *NCAM*, a marker for non-myelinating SCs, showed the same variable results (Fig. 2G). *SOX10* and *p75*, genes used as general Schwann cell markers, do not seem to be drastically affected by inhibitor treatment, and the effects vary between the different inhibitors and markers. Of note, both markers appear to be expressed more in

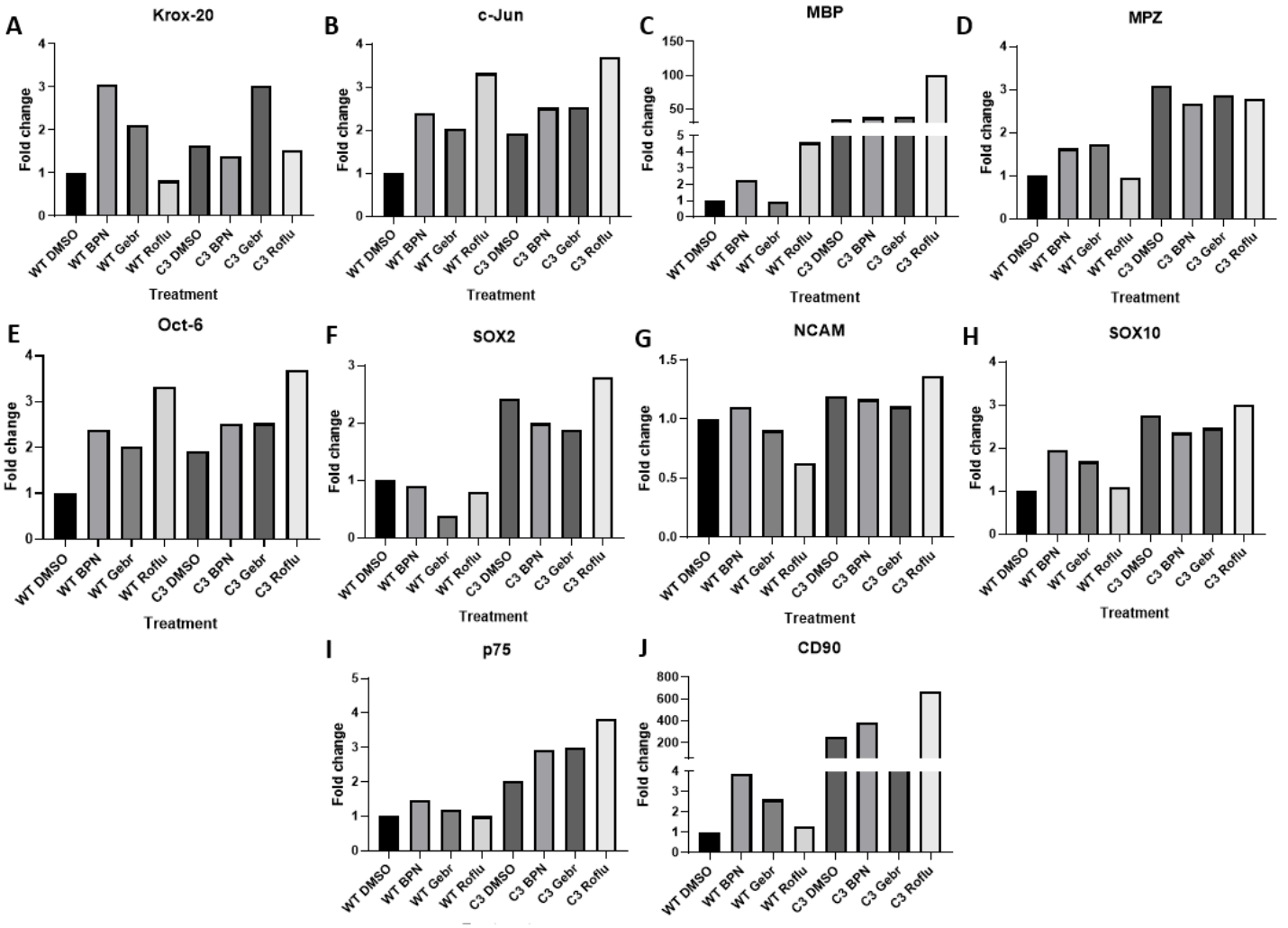

Fig. 2 – Schwann cell marker expression after PDE4(D) inhibition. WT and C3-PMP22 Schwann cells were treated for 6 days with either DMSO, 1 µM GEBR-32a (Gebr), 1 µM BPN14770 (BPN) or 1 µM Roflumilast (Roflu). Relative gene expression for several genes (A, *Krox-20*; B, *c-Jun*; C, *MBP*; D, *MPZ*; E, *Oct-6*; F, *SOX2*; G, *NCAM*; H, *SOX10*; I, *p75*; J, *CD90*) was quantified using qPCR. Note that N = 1 for every group. WT, wild type; C3, C3-PMP22. Data are represented as fold change relative to WT DMSO.

the C3-PMP22 cells than the WT cells (Fig. 2 H-I). Lastly, *CD90*, a fibroblast marker, was found to be expressed drastically higher in the C3-PMP22 cells compared to the WT cells, with GEBR-32a decreasing and Roflumilast increasing its expression in these cells. In the WT cells, the effects are smaller (Fig. 2J).

The effect of PDE4(D) inhibition on protein levels – To examine the effect of PDE4(D) inhibition on SC marker protein levels, WT and C3-PMP22 Schwann cells were seeded on glass coverslips and treated with inhibitors as previously mentioned. After the treatment period, samples were fluorescently stained for several markers (Fig. 3). For each condition, the integrated density of the fluorescent signal was calculated as a means of quantification. Note that n=1 for each condition, but 10 images were analyzed per coverslip. First, GFAP protein levels were investigated (Fig 3B). GFAP is expressed in dedifferentiated adult SCs, but not in myelinating SCs. When looking at the quantification, BPN ($p < 0.0001$) and Roflumilast ($p < 0.0001$) treatment significantly decrease the GFAP protein levels in C3-PMP22 SCs. Interestingly, GEBR-32a does not ($p = 0.0608$). Next, c-Jun protein levels were investigated (Fig.

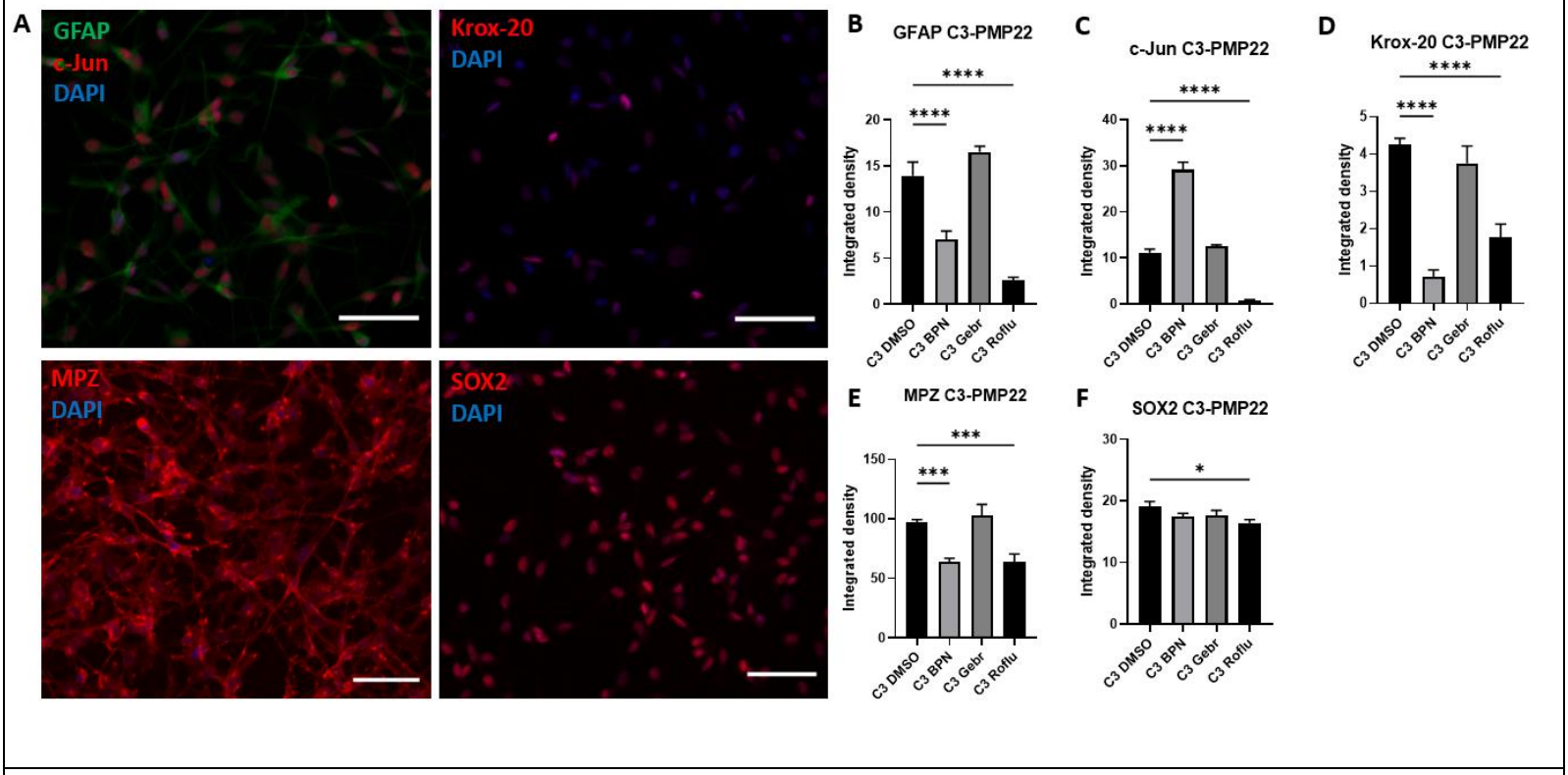

Fig. 3 – Immunostaining on C3-PMP22 Schwann cells after inhibitor treatment. (A) Representative images of C3-PMP22 Schwann cells stained for GFAP, c-Jun, Krox-20, MPZ, and SOX2. **(B-F)** Semi-quantitative analysis of the images using integrated density for GFAP **(B)**, c-Jun **(C)**, Krox-20 **(D)**, MPZ **(E)** and SOX2 **(F)**. For each condition, 10 photos were taken per coverslip, with 1 coverslip per condition (n = 1). Scale bar: 50µM. BPN, BPN14770, Gebr, GEBR-32a, Roflu, Roflumilast, C3, C3-PMP22. Data are presented as mean ± SEM. Statistical analysis: One-way ANOVA, Holm-Šídák multiple comparisons test. The means of all columns were compared to the control column (C3 DMSO). *p ≤ 0.05, **p ≤ 0.01, ***p ≤ 0.001, ****p ≤ 0.0001.

3C). Interestingly, BPN significantly increased c-Jun levels ($p < 0.0001$), while Roflumilast significantly decreased c-Jun levels ($p < 0.0001$). Again, GEBR-32a did not have a significant effect ($p = 0.2797$). When looking at Krox-20 (Fig. 3D), both BPN ($p < 0.0001$) and Roflumilast ($p < 0.0001$) significantly decreased protein levels, while GEBR-32a did not have a significant effect, although a small trend of decrease is visible ($p = 0.2606$). Then, when observing MPZ levels (Fig. 3E), again BPN ($p = 0.0006$) and Roflumilast ($p = 0.0006$) significantly decreased MPZ levels, while GEBR-32a did not show an effect ($p = 0.4894$). Lastly, only Roflumilast significantly decreased SOX2 levels ($p = 0.0364$), BPN ($p = 0.1989$) and GEBR-32a ($p = 0.1989$) had no significant effect (Fig. 3F).

GEBR-32a treatment improves motor function and nerve conduction in C3-PMP22 mice – To investigate the therapeutic effect of GEBR-32a *in vivo*, several functional aspects were investigated in the C3-PMP22 mouse model. 2 separate cohorts were analyzed: cohort A consists of 15 – 20 week-old mice at the start of the measurements, both male and female. Cohort B consists of only male 30 – 35 week-old mice. This was done to assess the effect of the treatment on different age groups. However, sample size is low in these cohorts (Cohort A: WT, n = 5; C3 Vehicle, n = 4; C3 Treated, n = 4; Cohort B: WT, n = 7, C3 Vehicle, n = 5, C3 Treated, n = 5). Therefore, both cohorts were also pooled in the analysis to generate a heterogenous population consisting of male and female mice of different ages, as well as higher statistical power (WT, n = 13; C3 Vehicle, n = 9; C3 Treated, n = 9). Mice were injected with either 0.3 mg/kg GEBR-32a or vehicle control (DMSO) twice per day. Before commencing treatment, baseline measurements for each functional assay were performed. Then, during week 3 of treatment,

these measurements were repeated. First, grip strength was quantified using a Newton meter, as well as the hanging wire test, which tests the animals' endurance to pull up their body weight (Fig. 4). At baseline, C3-PMP22 mice show a trend towards a lower maximum grip strength compared to WT mice in both age cohorts (Fig 4. A). When pooled, both C3-PMP22 groups show a significantly lower maximum grip strength compared to the WT group (Vehicle: p = 0.0057; Treated: p= 0.0265). During week 3 of treatment, maximum grip strength is notably lower compared to baseline across all groups. However, across both cohorts as well as the pooled cohorts, no significant differences were found between all groups (Fig. 4B). On the other hand, when testing endurance using the hanging wire test, at baseline, C3-PMP22 mice showed a significantly lower time before

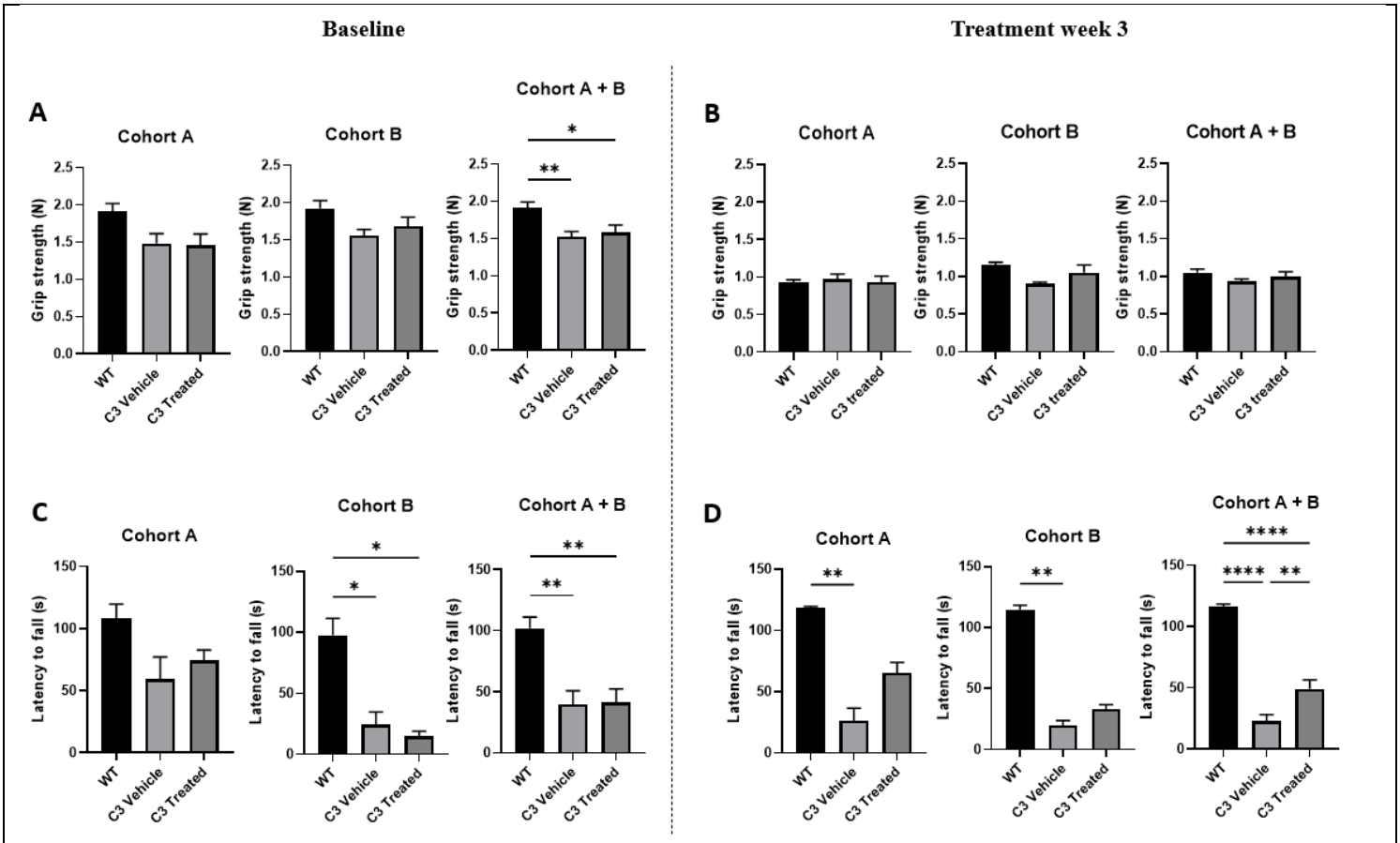

Fig. 4 – GEBR-32A treatment shows no conclusive effects on grip strength but increases grip endurance. (A, B) Maximum grip strength was recorded using a Newton meter. **(A)** Baseline measurements show no significant differences in grip strength between WT and C3 groups in Cohorts A and B. However, C3 mice show a trend towards worse performance compared to WT mice. When both cohorts are pooled, both C3 groups show a significantly lower grip strength compared to the WT group. **(B)** Measurements during week 3 of treatment. No significant differences were detected across all 3 cohorts. Of note, all mice performed notably worse compared to the baseline measurements. **(C, D)** Hanging wire test. Mice were placed on a cage lid and turned upside down. The time until falling was recorded. **(C)** Baseline measurements. In cohort B, both C3 groups showed significantly worse performance than the WT group, while in cohort A no significance was detected but a clear trend is seen. When both cohorts are pooled, both C3 groups perform significantly worse than the WT group. **(D)** Measurements during week 3 of treatment. After treatment, the untreated C3 group still performs significantly worse than the WT group, in contrast to the treated C3 group, which shows no significant difference. Furthermore, when both cohorts are pooled, the treated C3 group performs significantly better than the untreated C3 group. WT, wild type; C3 Vehicle, C3-PMP22 administered DMSO; C3 Treated, C3-PMP22 administered 0,3 mg/kg GEBR-32a. Data are presented as mean ± SEM. Statistical analysis: Kruskal-Wallis test, Dunn multiple comparisons test. *p ≤ 0.05, **p ≤ 0.01, ***p ≤ 0.001, ****p ≤ 0.0001.

falling compared to the WT group in cohort B (Vehicle: p = 0.0260; Treated: p = 0.0140) and the pooled cohorts (Vehicle: p = 0.0039; Treated: p = 0.0037) (Fig. 4C). In cohort A, the same trend is seen, but is not significant (Vehicle: p = 0.0927; Treated: p = 0.2537). After treatment, the untreated C3-PMP22 group still scored significantly lower than the WT group in both cohorts (Cohort A: p = 0.0070; Cohort B: p = 0.0023), but the treated C3-PMP22 groups did not differ significantly from the WT groups (Cohort A: p = 0.2848; Cohort B: p = 0.1101) (Fig. 4D). Furthermore, in the pooled cohorts, the treated group scores significantly better compared to the untreated group (p = 0.0046), although both C3-PMP2 groups scored significantly lower than the WT group (p < 0.0001). Secondly, endurance was tested using the Rotarod (Fig. 5). At baseline, C3-PMP22 mice scored significantly lower than the WT mice in cohort B (Vehicle: p < 0.0001; Treated: p < 0.0001), but not in cohort A (Vehicle: p = 0.1050; Treated: p = 0.0730), although a decreasing trend is seen. In the pooled cohorts, both C3-PMP22 groups scored significantly lower than the WT group (Vehicle: p = 0.0002; Treated: p = 0.0011) (Fig. 5A). After treatment, treated C3-PMP22 mice scored significantly better than the untreated group (Fig. 5B). In cohort A, the treated group showed a

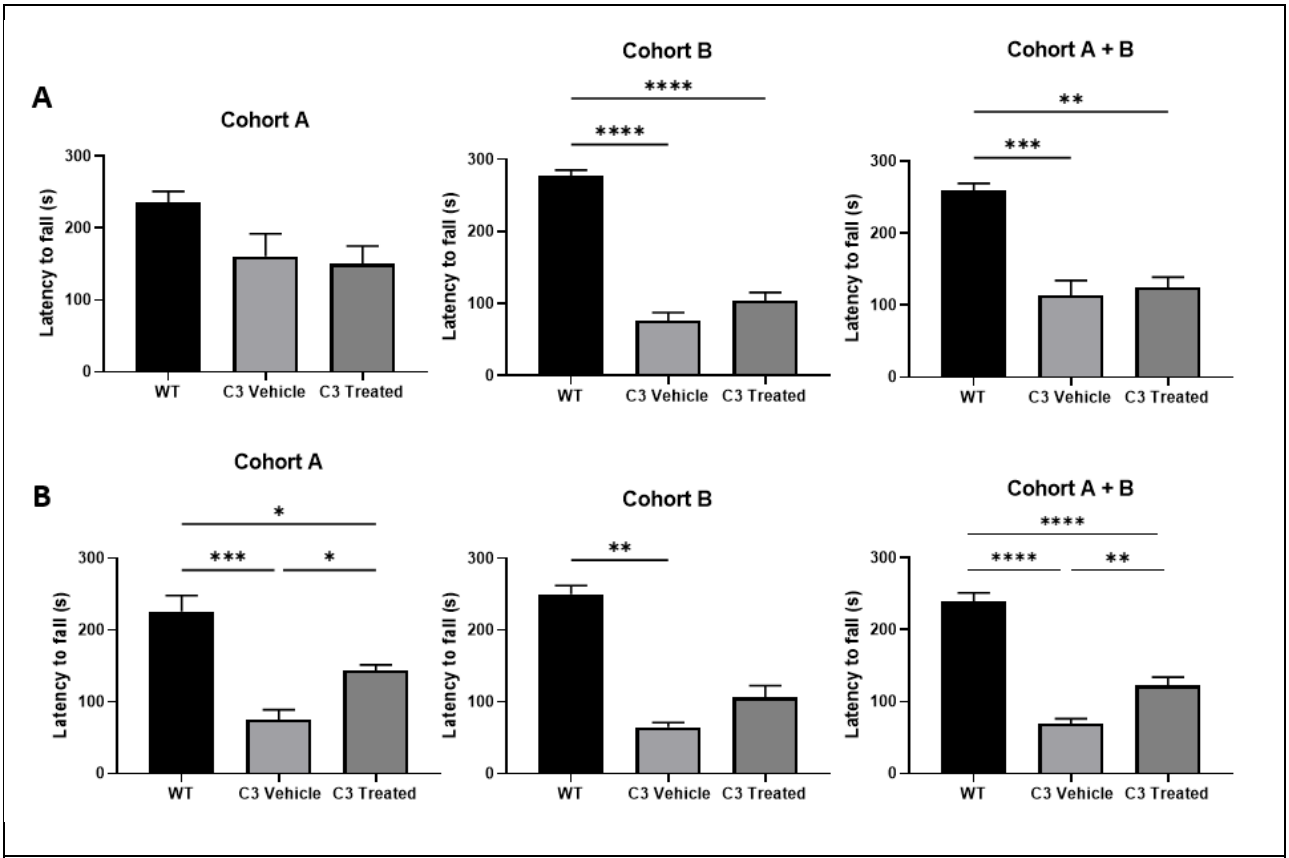

Fig. 5 – GEBR-32a treatment improves endurance on the Rotarod. Endurance was assessed using an accelerating protocol of 5 min. **(A)** Baseline measurements. In cohort B, both C3 groups perform significantly worse than the WT group. In cohort A, both C3 groups show a decreasing trend compared to the WT group, although no significance was detected. When both cohorts are pooled, both C3 groups perform significantly worse than the WT group. **(B)** Measurements during week 3 of treatment. After treatment, there is a significant improvement in the treated C3 group compared to the untreated C3 group in both cohort A and the pooled cohorts. In cohort B, there is a significant difference between the untreated C3 group and the WT group, but not between the treated C3 group and the WT group. WT, wild type; C3 Vehicle, C3-PMP22 administered DMSO; C3 Treated, C3-PMP22 administered 0,3 mg/kg GEBR-32a. Data are presented as mean ± SEM. Statistical analysis: Kruskal-Wallis test, Dunn multiple comparisons test. *p ≤ 0.05, **p ≤ 0.01, ***p ≤ 0.001, ****p ≤ 0.0001.

significantly higher endurance than the untreated group (p = 0.0221), despite still scoring significantly lower than the WT group (p = 0.0127). In cohort B, the treated group does not differ significantly from the WT group (p = 0913), while the untreated group scored significantly lower than the WT group (p = 0.0010). However, the treated group does not differ significantly from the untreated group (p = 0.5655). In the pooled cohorts, the treated group scores significantly higher than the untreated group (p = 0.0022), despite also scoring significantly lower than the WT group (p < 0.0001).

Next, motor coordination was evaluated using the grid walk, beam walk and pellet retrieval assays. First, sensorimotor function was assessed using the grid walk assay (Fig. 6A-B). Animals were allowed to traverse a wire grid and the number of hind paw slips was recorded (Suppl. Fig. 3). At baseline, both C3-PMP22 groups made significantly more foot

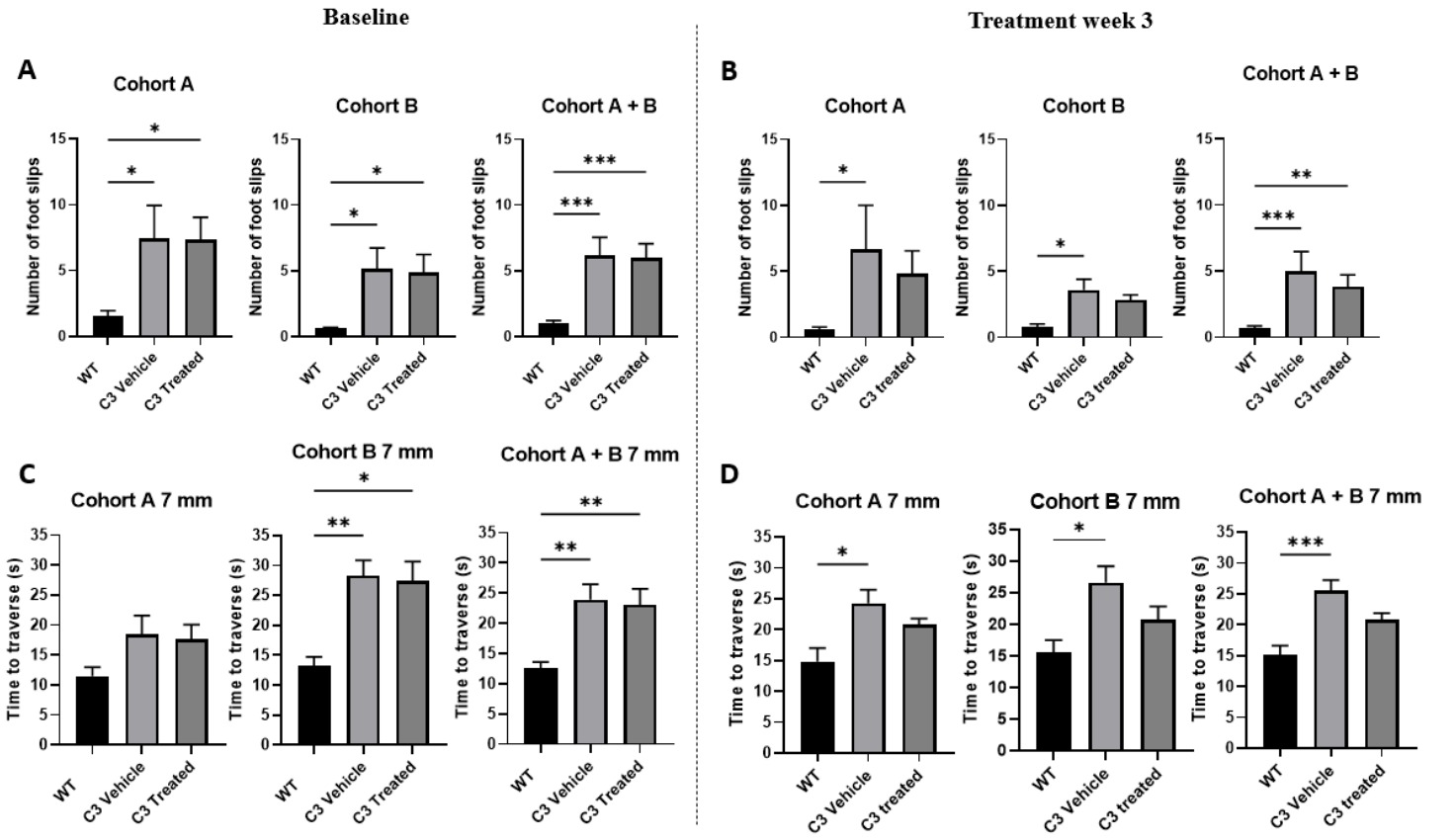

Fig. 6 – GEBR-32a treatment slightly improves sensorimotor coordination on the grid walk assay, as well as balance and coordination on the beam walk assay. (A, B) Grid walk assay. Mice traversed a wire grid and foot slips were recorded. **(A)** Baseline measurements. In both cohorts A and B, as well as the pooled cohort, C3 mice make significantly more foot slips compared to the WT group. **(B)** Measurements during week 3 of treatment. After treatment, the untreated C3 group makes significantly more foot slips than the WT group, while there is no significant difference between the treated C3 and WT groups in cohorts A and B. However, in the pooled cohorts, the treated C3 group does perform significantly worse than the WT group, although the p-value was higher than C3 treated vs WT. **(C, D)** Beam walk assay. Mice traversed a beam of 7 mm wide and 80 cm long, the time to traverse was recorded. **(C)** Baseline measurements. In cohort B, both C3 groups perform significantly worse than the WT group. In cohort A, the C3 groups show an increasing trend in traversing time. When both cohorts are pooled, both C3 groups perform significantly worse than the WT group. **(D)** Measurements during week 3 of treatment. Across all 3 cohorts, the untreated C3 group performs significantly worse than the WT group, while the treated C3 groups show no significant difference compared to the WT group. WT, wild type; C3 Vehicle, C3-PMP22 administered DMSO; C3 Treated, C3-PMP22 administered 0,3 mg/kg GEBR-32a. Data are presented as mean ± SEM. Statistical analysis: Kruskal-Wallis test, Dunn multiple comparisons test. *p ≤ 0.05, **p ≤ 0.01, ***p ≤ 0.001.

slips compared to the WT group in both cohort A (Vehicle: p = 0.0420; Treated: p = 0.0320) and cohort B (Vehicle: p = 0.0101; Treated: p = 0.0126), as well as the pooled cohorts (Vehicle: p = 0.0006; Treated: p = 0.0005) (Fig. 6A). However, after treatment, in cohorts A and B, the untreated C3-PMP22 group still performs significantly worse than the WT group (Cohort A: p = 0.0179; Cohort B: p = 0.0208), while the treated C3-PMP22 group does not differ significantly from the WT group (Cohort A: p = 0.0701; Cohort B: p = 0.0776). When both cohorts are pooled, both C3-PMP22 groups still perform significantly worse than the WT group, although the p-value is higher in the treated group (Vehicle: p = 0.0003; Treated: p = 0.0020) (Fig. 6B). However, there is no significant difference between the treated and untreated C3-PMP22 groups across all cohorts (Cohort A: p > 0.9999; Cohort B: p > 0.9999; Cohort A + B: p > 0.9999). Secondly, balance and coordination were examined using the beam walk assay (Fig. 6C-D). Animals traversed a wooden beam of 7 mm wide and 80 cm long, and the time taken to traverse was recorded. At baseline, both C3-PMP22 groups took significantly longer to traverse the beam than the WT group in cohort B (Vehicle: p = 0.0069; Treated: p = 0.0203), but not cohort A (Vehicle: p = 0.2806; Treated: p = 0.4518). When pooled, both C3-PMP22 groups took significantly longer than the WT group to traverse the beam (Vehicle: p = 0.0031; Treated: p = 0.0086) (Fig. 6C). After treatment, the untreated C3-PMP22 group still took significantly longer than the WT group to traverse across all cohorts (Cohort A: p = 0.0468; Cohort B: p = 0.0120; Cohort A + B: p = 0.0003), but the treated group did not differ significantly from the

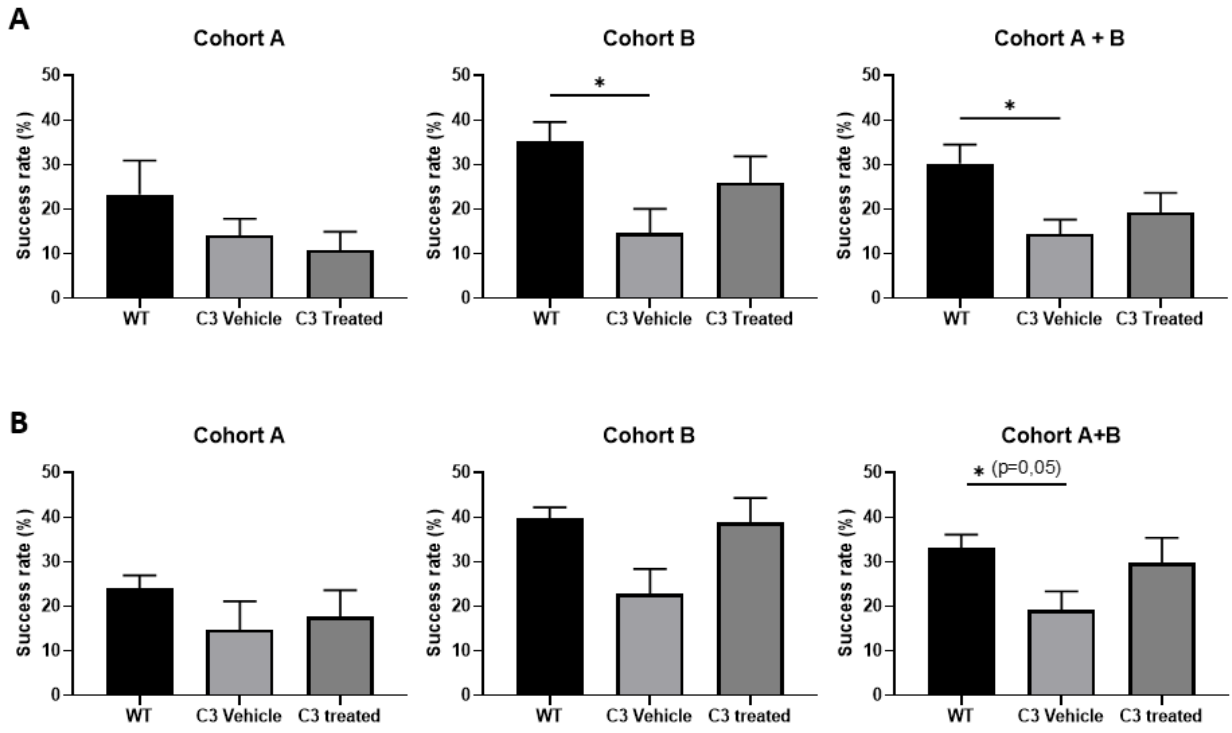

Fig. 7 – GEBR-32a treatment improves motor coordination in the pellet retrieval task. 30 reaching attempts were recorded per animal and the success rate was calculated. **(A)** Baseline measurements. In cohort B and the pooled cohorts, the untreated group scored significantly worse than the WT group. In cohort A, there is a decreasing trend in the C3 groups. **(B)** Measurements during week 3 of treatment. Treated C3 mice show an improving trend compared to the untreated C3 mice across all cohorts. In the pooled cohorts, untreated C3 mice perform significantly worse than the WT mice, while the treated C3 mice do not differ from the WT group. WT, wild type; C3 Vehicle, C3-PMP22 administered DMSO; C3 Treated, C3-PMP22 administered 0,3 mg/kg GEBR-32a. Data are presented as mean ± SEM. Statistical analysis: Kruskal-Wallis test, Dunn multiple comparisons test. *p ≤ 0.05.

WT group across all cohorts (Cohort A: p = 0.0.8475; Cohort B: p = 0.7488; Cohort A + B: p = 0.2166), indicating functional improvement in the treated C3-PMP22 group (Fig. 6D). However, no significant differences were found between the treated and untreated C3-PMP22 groups across all cohorts (Cohort A; p = 0.6075; Cohort B: p = 0.3296; Cohort A + B: p = 0.1609). The beam walk assay was also performed using beams of 18 and 12 mm wide (Suppl. Fig. 2, 5). However, no significant effects were detected here (Suppl. Fig. 5).

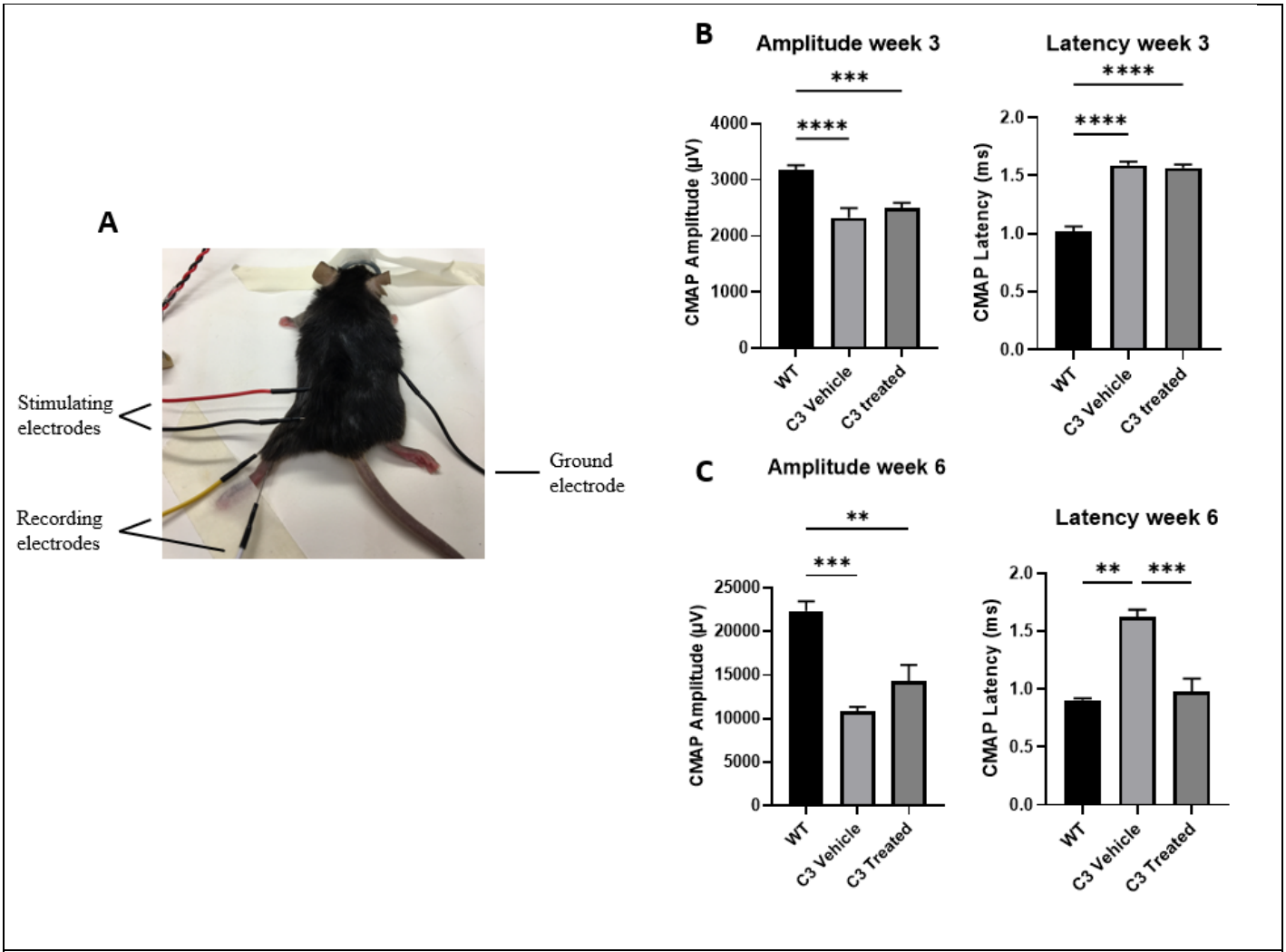

Fig. 8 – GEBR-32a treatment significantly decreases CMAP latency but does not increase CMAP amplitude. Compound muscle action potentials (CMAPs) were recorded for the sciatic nerve of each animal. Cohorts A and B were pooled for these measurements. **(A)** Photo of the setup, with the simulating, recording and ground electrodes indicated. **(B)** Measurements during week 3 of treatment. The sciatic nerve was stimulated at 2,5 and 8 mA in WT and C3-PMP22 mice, respectively. Both C3 groups show a significantly lower CMAP amplitude and higher latency than the WT group, with no significant difference between the untreated and treated groups. **(C)** Measurements during week 6 of treatment. Here sciatic nerves were supramaximally stimulated. Both C3 groups show a significantly lower amplitude than the WT group, with no significant difference between the untreated and treated groups. However, an increasing trend is seen in the treated group compared to the untreated group. Next, the treated C3-PMP22 group shows a significantly lower latency compared to the untreated C3-PMP22 group. The treated group does not differ significantly from the WT group, while the untreated group shows a significantly higher latency than the WT group. WT, wild type; C3 Vehicle, C3-PMP22 administered DMSO; C3 Treated, C3-PMP22 administered 0,3 mg/kg GEBR-32a. Data are presented as mean ± SEM. Statistical analysis: Kruskal-Wallis test, Dunn multiple comparisons test. *p ≤ 0.05, **p ≤ 0.01, ***p ≤ 0.001, ****p ≤ 0.0001.

Third, front paw coordination was investigated using the pellet retrieval task (Fig. 7). After a training period, mice were able to reach for a food pellet from within a plastic container through a slit. 30 reaching attempts were recorded and the rate of successfully grabbing and feeding the pellet into the mouth was calculated (Suppl. Fig. 4). It is important to note that at baseline, the untreated C3-PMP22 group scored significantly lower than the WT group in cohort B ($p = 0.0396$) and the pooled cohorts ($p = 0.0316$), while the treated C3-PMP22 groups did not differ significantly from the WT groups (Cohort B: $p = 0.9747$; Cohort A + B: $p = 0.3226$). In cohort A, all groups did not differ significantly from each other (Fig. 7A). After treatment, all groups did not differ from each other in cohorts A and B (Fig. 7B). When pooled, the untreated C3-PMP22 group scored almost significantly worse than the WT group ($p = 0.0528$), while the treated C3-PMP22 group did not differ from the WT group ($p > 0.9999$).

Lastly, nerve conduction was quantified using electrophysiological measurements (Fig. 8). These measurements were recorded during week 3 of treatment and mice from both cohorts were pooled. Mice were anesthetized and the proximal sciatic nerve was stimulated with either 2,5 mA or 8 mA pulses, for WT and C3-PMP22 mice, respectively. The response, compound muscle action potentials (CMAPs), were recorded in the distal hind limb muscle tissue (Fig 8A). Axonal integrity was assessed by quantifying the amplitude of the CMAPs. Both C3-PMP22 groups had a significantly lower amplitude compared to the WT animals (Vehicle: $p < 0.0001$; Treated: $p = 0.0004$), while treatment did not result in a significant difference with the untreated group ($p = 0.5761$) (Fig. 8B). Furthermore, conduction speed was examined by quantifying the CMAP latency after stimulation. Both C3-PMP22 groups showed a significantly higher latency than the WT group (Vehicle: $p < 0.0001$; Treated: $p < 0.0001$), while treatment did not result in a significant improvement compared to the untreated group ($p = 0.9041$). However, as significant improvements were observed in the behavioral assays but not the electrophysiological measurements, we opted to continue treating the mice and repeating the electrophysiological measurements during week 6 of treatment. Here the sciatic nerve was supramaximally stimulated to record the maximal CMAP response (Fig. 8C). When looking at the CMAP amplitude, there was still no significant difference between the untreated and treated C3-PMP22 groups ($p > 0.9999$). However, an increasing trend is seen in the treated group. On the other hand, the treated C3-PMP22 group showed a significantly lower latency compared to the untreated C3-PMP22 group ($p = 0.0002$), to the point where the treated group does not differ from the WT group ($p = 0.6754$).

DISCUSSION

This study aimed to assess the therapeutic potential of PDE4D inhibition in CMT1A. We found that treatment with the PDE4D-specific inhibitor GEBR-32a significantly improved motor function in the C3-PMP22 mouse model. Furthermore, electrophysiological measurements revealed a significant increase in sciatic nerve conduction speed after treatment, indicating a boost in peripheral myelination. However, the *in vitro* data on the differentiation state of treated SCs remain inconclusive.

We showed that all isoforms of PDE4D showed an increasing trend in expression in C3-PMP22 SCs compared to WT SCs. This could result in an intrinsically lower cAMP level compared to WT SCs and confirms PDE4D as a viable target to increase cAMP content in CMT1A. In fact, lower cAMP levels were already observed in CMT1A rat SCs compared to WT rat SCs (33). These findings further confirm that the use of cAMP-increasing agents can prove beneficial to restore the myelinating SC phenotype.

Next, our findings on PDE4D inhibition affecting the SC differentiation state *in vitro* are inconclusive. First of all, it is important to note that both the qPCR and immunocytochemistry experiments were performed with a sample size of 1 for each condition, so no conclusive findings can be formulated. These experiments need to be repeated with a higher sample size in order to accurately examine the effect of the different inhibitors *in vitro*. However, some first observations can be made based on the trends seen in these experiments. Besides GEBR-32a, another PDE4D-specific inhibitor, BPN14770 (BPN), was investigated for comparison, as well as the PDE4 pan-inhibitor Roflumilast, an FDA-approved compound for use against COPD (34). BPN is an allosteric inhibitor of PDE4D, while GEBR-32a

directly interacts with the catalytic domain of PDE4D (35-37). When looking at the two main positive and negative transcriptional regulators of myelination, we expected PDE4(D) inhibition to increase *Krox-20* and decrease *c-Jun* expression. An increase in *Krox-20* expression was observed in C3-PMP22 cells treated with GEBR-32a, but not BPN or Roflumilast. This could indicate that GEBR-32a treatment can stimulate differentiation to the myelinating phenotype through elevation of *Krox-20* expression. However, when looking at *c-Jun*, all 3 inhibitors slightly increased its expression, with Roflumilast having the most profound effect. This is the opposite of what was expected. However, if this effect is confirmed, it could indicate that PDE4D-specific inhibition results in a smaller increase in *c-Jun* expression compared to PDE4 inhibition, as BPN and GEBR-32a show a smaller increase than Roflumilast. Next, when investigating the myelin proteins *MPZ* and *MBP*, we expected the expression of both genes to increase upon treatment to indicate differentiation to the myelinating phenotype. Interestingly, the C3-PMP22 cells showed a higher expression compared to the WT cells, especially *MBP*. The inhibitors did not appear to have an effect, except Roflumilast which increased *MBP* expression. Additionally, we investigated *Oct-6* and *SOX2*, another example of positive and negative transcriptional regulators of myelination, respectively (38, 39). Here, we expected an increase in *Oct-6* and a decrease in *SOX2* expression. All 3 inhibitors appeared to increase the expression of *Oct-6*, with Roflumilast having the largest effect. This indicates an boost in differentiation. On the other hand, GEBR-32a appeared to decrease *SOX2* expression, while Roflumilast appeared to increase its expression. There was no apparent effect of BPN. It is noteworthy that all C3-PMP22 groups showed a higher expression of *SOX2* compared to the WT groups, indicating that these cells might be in a dedifferentiated or non-myelinating state. However, *NCAM*, a marker for non-myelinating SCs, showed no apparent differences in expression across all groups (40). Next, *SOX10* and *p75*, proteins generally used as SC markers, were investigated (41, 42). Here, there was no apparent effect of the inhibitors on *SOX10* expression, while all 3 inhibitors appeared to slightly increase *p75* expression in C3-PMP22 cells. It is noteworthy that the C3-PMP22 cells showed a higher expression of both *SOX10* and *p75*. However, most notably, C3-PMP22 cells showed a drastically higher expression of *CD90*, a marker expressed by fibroblasts, but not SCs (43). This might indicate contamination of the C3-PMP22 culture with fibroblasts, rendering the aforementioned results unusable. Interestingly, several SC markers also showed a higher expression in the C3-PMP22 cells. Another suggested reason can be a technical mistake during RNA isolation or qPCR. In conclusion, while some observations were made, these experiments need to be repeated on new cell cultures, preferably cultures where SC identity and purity was confirmed. These experiments should consist of at least 3 biological replicates, as opposed to the 1 used in this study.

Likewise, our observations on the effect of PDE4(D) inhibition on protein levels are inconclusive. Again, it is important to note that the immunocytochemistry was performed with a sample size of 1 for each condition, and need to be repeated. First, we examined the protein levels of GFAP, an intermediate filament expressed in non-myelinating adult SCs, but not myelinating adult SCs (44). Here, BPN and Roflumilast significantly decreased GFAP protein levels in C3-PMP22 SCs, indicating a myelinating phenotype, while GEBR-32a showed no significant effect. Interestingly, BPN treatment appears to have an opposite effect than what was expected, both increasing c-Jun and decreasing Krox-20 and MPZ levels. Roflumilast decreased c-Jun levels but also decreased Krox-20 and MPZ levels. Lastly, there were no large effects on SOX2 levels, with the exception of Roflumilast significantly decreasing them. Across these proteins, GEBR-32a surprisingly showed no effects. Taken together, these data show no conclusive effects and as the qPCR experiments, these experiments need to be repeated on new cell cultures, with at least 3 biological replicates per condition. Previous studies revealed that the broad-spectrum PDE inhibitor IBMX, as well as the PDE3 inhibitor cilostazol, significantly promote SC differentiation *in vitro* (45, 46). Therefore, we expect PDE4(D) inhibition to significantly boost SC differentiation to the myelinating phenotype *in vitro*, as was also indicated by functional repair after PDE4D inhibition *in vivo*. Furthermore, it might be possible to increase the concentration of the inhibitors used in both *in vitro* experiments. For

example, GEBR-32 showed no toxic effects even at concentrations as high as 100 µM (24).

To assess the effect of PDE4D inhibition on CMT1A symptoms *in vivo*, we opted to investigate the therapeutic potential of GEBR-32a, as this is a novel compound with a promising therapeutic profile. Moreover, it inhibits practically every isoform of PDE4D, as opposed to BPN14770, which is only selective for PDE4D3 and PDE4D7 (37, 47). To our knowledge, PDE4D-selective inhibition has never been attempted before as a therapeutic strategy for CMT1A. However, previous research demonstrated that PDE4 inhibition by Rolipram enhanced myelination *in vivo* when combined with SC transplantation after spinal cord injury (48, 49). Moreover, Rolipram also promoted remyelination in the central nervous system in a multiple sclerosis model (23). This led us to believe that PDE4D-specific inhibition could show the same therapeutic potential in the peripheral nervous system without the side effects commonly seen with PDE4 inhibition (24, 25). Our *in vivo* study showed very promising results of GEBR-32a treatment in C3-PMP22 mice. First, GEBR-32a treatment significantly improved endurance, both in the strength-based hanging wire test and the movement-based Rotarod test. Secondly, motor coordination was also significantly improved, as indicated by an improvement in sensorimotor function on the grid walk assay, balance and coordination on the beam walk assay, and forelimb coordination on the pellet retrieval task. Taken together, these data form evidence that PDE4D inhibition by GEBR-32a can improve motor function in CMT1A mice. However, an interesting difference between endurance and coordination can be seen. In the hanging wire and rotarod assays, GEBR-32a treatment does not appear to increase endurance, but rather prevent a decline in endurance over time. This is indicated by the treated C3-PMP22 mice staying at approximately the same level compared to baseline, while the untreated C3-PMP22 mice perform worse compared to baseline. This effect can already be observed when comparing cohorts A and B at baseline, where the older C3-PMP22 animals in cohort B appeared to perform worse than the younger animals in cohort A. On the other hand, coordination does appear to be directly improved by treatment, as indicated by the untreated C3-PMP22 group performing at approximately the same level compared to baseline in the grid walk, beam walk and pellet retrieval assays. Based on these findings, a subsequent step can be to start treating mice at an early age in order to get optimal results. In humans, CMT1A symptoms develop in the first 2 decades of life, but disease progression was observed in adult patients (28). Therefore, starting therapy as early as possible could be the best way to both improve motor coordination and prevent a decline in endurance.

Secondly, the significant improvements in motor function are accompanied by a spectacular increase in nerve conduction velocity, as indicated by the decrease in sciatic nerve CMAP latency in C3-PMP22 mice to the same level as WT mice in week 6 of treatment. We did not observe any significant effects on nerve conduction during week 3 when we stimulated the sciatic nerve using a set current. However, because significant improvements in motor function were observed, we opted to continue the treatment and repeat the electrophysiological measurements. In week 6, we stimulated the sciatic nerve until a maximal response was recorded, and here a significant effect of treatment was detected. These findings indicate that GEBR-32a treatment improves motor function through the enhancement of nerve conduction speed. Presumably, this effect is due to an enhancement in myelination, but this needs to be confirmed by post-mortem tissue analysis. On the other hand, GEBR-32a inhibition did not appear to increase CMAP amplitude, which would indicate an increase in axonal integrity. However, after six weeks an increasing trend is seen in the treated C3-PMP22 group. This could mean that this effect is slower.

The next step in this research is to repeat the functional assays during week 7 of treatment to investigate whether prolonged treatment further improves motor function. At the end of week 7, the animals will be sacrificed for tissue analysis. Here, sciatic nerves and brachial plexuses will be isolated and examined using transmission electron microscopy and immunocytochemistry to determine the myelination state of these nerve fibers. Ultimately, the next steps could be to investigate commencing treatment at an early age, as well as determine the optimal dose of GEBR-32a for maximal therapeutic effect while minimizing unwanted side effects. Additionally, CMAP amplitude can be investigated during prolonged treatment to confirm whether there is an effect of

treatment on axonal integrity. Furthermore, as *PMP22* overexpression results in increased Ca^{2+} influx through upregulation of the P2X7 receptor, it was shown that blocking of P2X7 decreased intracellular Ca2+ levels and improved myelination *in vitro*, while also slightly increasing cAMP levels (33). Moreover, another study confirmed that P2X7 inhibition improves myelination in a CMT1A rat model (50). Regardless, this study observed a decrease in muscle strength at high doses, possibly due to the P2X7 receptor playing a role in neuronal synaptic transmission and its expression in skeletal muscle tissue, decreasing Ca^{2+} influx in the muscle upon inhibition (50-52). Thus, it might be interesting to investigate a combination of PDE4D inhibition with P2X7 inhibition at a low dose *in vivo* to maximize the effect of both compounds.

CONCLUSION

In conclusion, PDE4D is a promising therapeutic target for the treatment of CMT1A. Furthermore, the PDE4D-specific inhibitor GEBR-32a has shown to be of great interest for further investigation, as GEBR-32a treatment significantly alleviated both functional and electrophysiological symptoms of CMT1A. However, the exact molecular mechanisms of PDE4D inhibition stimulating functional repair need to be further examined. The *in vitro* data presented in this study are inconclusive. Additionally, these data are based on a sample size of 1 and are therefore not suitable to draw any conclusions. The next steps in validating PDE4D inhibition as a treatment for CMT1A include repeating the *in vitro* experiments with appropriate sample sizes, as well as post-mortem tissue analysis on the mice used in this study. In the future, GEBR-32a can be further investigated and developed as a promising therapy for CMT1A, possibly in combination with other therapeutic compounds.

REFERENCES

1. Barreto LCLS, Oliveira FS, Nunes PS, de França Costa IMP, Garcez CA, Goes GM, et al. Epidemiologic Study of Charcot-Marie-Tooth Disease: A Systematic Review. Neuroepidemiology. 2016;46(3):157-65.
2. Morena J, Gupta A, Hoyle JC. Charcot-Marie-Tooth: From Molecules to Therapy. International journal of molecular sciences. 2019;20(14):3419.
3. Saporta ASD, Sottile SL, Miller LJ, Feely SME, Siskind CE, Shy ME. Charcot-Marie-Tooth disease subtypes and genetic testing strategies. Ann Neurol. 2011;69(1):22-33.
4. Li J, Parker B, Martyn C, Natarajan C, Guo J. The PMP22 gene and its related diseases. Mol Neurobiol. 2013;47(2):673-98.
5. Morell P QR. The Myelin Sheath. In: al. SGe, editor. Basic Neurochemistry: Molecular, Cellular and Medical Aspects, 6th edition. Philadelphia: Lippincott-Raven; 1999.
6. Pereira JA, Lebrun-Julien F, Suter U. Molecular mechanisms regulating myelination in the peripheral nervous system. Trends Neurosci. 2012;35(2):123-34.
7. Soto J, Monje PV. Axon contact-driven Schwann cell dedifferentiation. Glia. 2017;65(6):864-82.
8. Kim JK, Lee HJ, Park HT. Two faces of Schwann cell dedifferentiation in peripheral neurodegenerative diseases: pro-demyelinating and axon-preservative functions. Neural Regen Res. 2014;9(22):1952-4.
9. Bai Y, Zhang X, Katona I, Saporta MA, Shy ME, O'Malley HA, et al. Conduction block in PMP22 deficiency. J Neurosci. 2010;30(2):600-8.
10. Guo J, Wang L, Zhang Y, Wu J, Arpag S, Hu B, et al. Abnormal junctions and permeability of myelin in PMP22-deficient nerves. Ann Neurol. 2014;75(2):255-65.

11. Giambonini-Brugnoli G, Buchstaller J, Sommer L, Suter U, Mantei N. Distinct disease mechanisms in peripheral neuropathies due to altered peripheral myelin protein 22 gene dosage or a Pmp22 point mutation. Neurobiol Dis. 2005;18(3):656-68.
12. Vigo T, Nobbio L, Hummelen PV, Abbruzzese M, Mancardi G, Verpoorten N, et al. Experimental Charcot–Marie–Tooth type 1A: A cDNA microarrays analysis. Molecular and Cellular Neuroscience. 2005;28(4):703-14.
13. Nobbio L, Sturla L, Fiorese F, Usai C, Basile G, Moreschi I, et al. P2X7-mediated increased intracellular calcium causes functional derangement in Schwann cells from rats with CMT1A neuropathy. J Biol Chem. 2009;284(34):23146-58.
14. Fortun J, Go JC, Li J, Amici SA, Dunn WA, Notterpek L. Alterations in degradative pathways and protein aggregation in a neuropathy model based on PMP22 overexpression. Neurobiol Dis. 2006;22(1):153-64.
15. Bacallao K, Monje PV. Requirement of cAMP signaling for Schwann cell differentiation restricts the onset of myelination. PloS one. 2015;10(2):e0116948-e.
16. Monje PV, Athauda G, Wood PM. Protein kinase A-mediated gating of neuregulin-dependent ErbB2-ErbB3 activation underlies the synergistic action of cAMP on Schwann cell proliferation. J Biol Chem. 2008;283(49):34087-100.
17. Jessen KR, Mirsky R. Negative regulation of myelination: relevance for development, injury, and demyelinating disease. Glia. 2008;56(14):1552-65.
18. Jessen KR, Mirsky R, Morgan L. Role of cyclic AMP and proliferation controls in Schwann cell differentiation. Annals of the New York Academy of Sciences. 1991;633:78-89.
19. Monje PV, Soto J, Bacallao K, Wood PM. Schwann cell dedifferentiation is independent of mitogenic signaling and uncoupled to proliferation: role of cAMP and JNK in the maintenance of the differentiated state. J Biol Chem. 2010;285(40):31024-36.
20. Guo L, Moon C, Niehaus K, Zheng Y, Ratner N. Rac1 controls Schwann cell myelination through cAMP and NF2/merlin. J Neurosci. 2012;32(48):17251-61.
21. Schmid D, Zeis T, Schaeren-Wiemers N. Transcriptional regulation induced by cAMP elevation in mouse Schwann cells. ASN Neuro. 2014;6(3):137-57.
22. Azevedo MF, Faucz FR, Bimpaki E, Horvath A, Levy I, de Alexandre RB, et al. Clinical and molecular genetics of the phosphodiesterases (PDEs). Endocr Rev. 2014;35(2):195-233.
23. Syed YA, Baer A, Hofer MP, González GA, Rundle J, Myrta S, et al. Inhibition of phosphodiesterase-4 promotes oligodendrocyte precursor cell differentiation and enhances CNS remyelination. EMBO Mol Med. 2013;5(12):1918-34.
24. Ricciarelli R, Brullo C, Prickaerts J, Arancio O, Villa C, Rebosio C, et al. Memory-enhancing effects of GEBR-32a, a new PDE4D inhibitor holding promise for the treatment of Alzheimer's disease. Scientific reports. 2017;7:46320-.
25. Ricciarelli R, Fedele E. Phosphodiesterase 4D: an enzyme to remember. Br J Pharmacol. 2015;172(20):4785-9.
26. Monje PV, Sant D, Wang G. Phenotypic and Functional Characteristics of Human Schwann Cells as Revealed by Cell-Based Assays and RNA-SEQ. Mol Neurobiol. 2018;55(8):6637-60.
27. Bruno O, Fedele E, Prickaerts J, Parker LA, Canepa E, Brullo C, et al. GEBR-7b, a novel PDE4D selective inhibitor that improves memory in rodents at non-emetic doses. Br J Pharmacol. 2011;164(8):2054-63.

28. Verhamme C, King RHM, ten Asbroek ALMA, Muddle JR, Nourallah M, Wolterman R, et al. Myelin and Axon Pathology in a Long-Term Study of PMP22-Overexpressing Mice. Journal of Neuropathology & Experimental Neurology. 2011;70(5):386-98.
29. Andersen ND, Monje PV. Isolation, Culture, and Cryopreservation of Adult Rodent Schwann Cells Derived from Immediately Dissociated Teased Fibers. Methods Mol Biol. 2018;1739:49-66.
30. Hantke J, Carty L, Wagstaff LJ, Turmaine M, Wilton DK, Quintes S, et al. c-Jun activation in Schwann cells protects against loss of sensory axons in inherited neuropathy. Brain. 2014;137(Pt 11):2922-37.
31. Chen C-C, Gilmore A, Zuo Y. Study motor skill learning by single-pellet reaching tasks in mice. J Vis Exp. 2014(85):51238.
32. Au - Pollari E, Au - Prior R, Au - Robberecht W, Au - Van Damme P, Au - Van Den Bosch L. In Vivo Electrophysiological Measurement of Compound Muscle Action Potential from the Forelimbs in Mouse Models of Motor Neuron Degeneration. JoVE. 2018(136):e57741.
33. Nobbio L, Visigalli D, Mannino E, Fiorese F, Kassack MU, Sturla L, et al. The Diadenosine Homodinucleotide P18 Improves In Vitro Myelination in Experimental Charcot-Marie-Tooth Type 1A. Journal of Cellular Biochemistry. 2014;115(1):161-7.
34. Yu T, Fain K, Boyd CM, Singh S, Weiss CO, Li T, et al. Benefits and harms of roflumilast in moderate to severe COPD. Thorax. 2014;69(7):616-22.
35. Wang Y, Gao S, Zheng V, Chen L, Ma M, Shen S, et al. A Novel PDE4D Inhibitor BPN14770 Reverses Scopolamine-Induced Cognitive Deficits via cAMP/SIRT1/Akt/Bcl-2 Pathway. Frontiers in cell and developmental biology. 2020;8:599389-.
36. Zhang C, Xu Y, Chowdhary A, Fox D, 3rd, Gurney ME, Zhang HT, et al. Memory enhancing effects of BPN14770, an allosteric inhibitor of phosphodiesterase-4D, in wild-type and humanized mice. Neuropsychopharmacology : official publication of the American College of Neuropsychopharmacology. 2018;43(11):2299-309.
37. Cavalloro V, Russo K, Vasile F, Pignataro L, Torretta A, Donini S, et al. Insight into GEBR-32a: Chiral Resolution, Absolute Configuration and Enantiopreference in PDE4D Inhibition. Molecules. 2020;25(4):935.
38. Jaegle M, Meijer D. Role of Oct-6 in Schwann cell differentiation. Microscopy research and technique. 1998;41(5):372-8.
39. Roberts SL, Dun XP, Doddrell RDS, Mindos T, Drake LK, Onaitis MW, et al. Sox2 expression in Schwann cells inhibits myelination in vivo and induces influx of macrophages to the nerve. Development (Cambridge, England). 2017;144(17):3114-25.
40. Roche PH, Figarella-Branger D, Daniel L, Bianco N, Pellet W, Pellissier JF. Expression of cell adhesion molecules in normal nerves, chronic axonal neuropathies and Schwann cell tumors. Journal of the neurological sciences. 1997;151(2):127-33.
41. Finzsch M, Schreiner S, Kichko T, Reeh P, Tamm ER, Bösl MR, et al. Sox10 is required for Schwann cell identity and progression beyond the immature Schwann cell stage. The Journal of cell biology. 2010;189(4):701-12.
42. Gonçalves NP, Mohseni S, El Soury M, Ulrichsen M, Richner M, Xiao J, et al. Peripheral Nerve Regeneration Is Independent From Schwann Cell p75(NTR) Expression. Frontiers in cellular neuroscience. 2019;13:235-.
43. Kisselbach L, Merges M, Bossie A, Boyd A. CD90 Expression on human primary cells and elimination of contaminating fibroblasts from cell cultures. Cytotechnology. 2009;59(1):31-44.

44. Triolo D, Dina G, Lorenzetti I, Malaguti M, Morana P, Del Carro U, et al. Loss of glial fibrillary acidic protein (GFAP) impairs Schwann cell proliferation and delays nerve regeneration after damage. Journal of Cell Science. 2006;119(19):3981-93.
45. Koyanagi M, Imai S, Iwamitsu Y, Matsumoto M, Saigo M, Moriya A, et al. Cilostazol is an effective causal therapy for preventing paclitaxel-induced peripheral neuropathy by suppression of Schwann cell dedifferentiation. Neuropharmacology. 2021;188:108514.
46. Morgan L, Jessen KR, Mirsky R. The effects of cAMP on differentiation of cultured Schwann cells: progression from an early phenotype (04+) to a myelin phenotype (P0+, GFAP-, N-CAM-, NGF-receptor-) depends on growth inhibition. The Journal of cell biology. 1991;112(3):457-67.
47. BPN14770. In: Adooq Bioscience. 2021. Available from: https://www.adooq.com/bpn14770.html?gclid=Cj0KCQjw8IaGBhCHARIsAGIRRYotNfhhTZo733Th0HHV4x1ksjirw8JKk4BSfWvdSDHAOGBZe-Fp4m0aAhzmEALw_wcB
48. Pearse DD, Pereira FC, Marcillo AE, Bates ML, Berrocal YA, Filbin MT, et al. cAMP and Schwann cells promote axonal growth and functional recovery after spinal cord injury. Nature medicine. 2004;10(6):610-6.
49. Flora G, Joseph G, Patel S, Singh A, Bleicher D, Barakat DJ, et al. Combining neurotrophin-transduced schwann cells and rolipram to promote functional recovery from subacute spinal cord injury. Cell transplantation. 2013;22(12):2203-17.
50. Sociali G, Visigalli D, Prukop T, Cervellini I, Mannino E, Venturi C, et al. Tolerability and efficacy study of P2X7 inhibition in experimental Charcot-Marie-Tooth type 1A (CMT1A) neuropathy. Neurobiol Dis. 2016;95:145-57.
51. Deuchars SA, Atkinson L, Brooke RE, Musa H, Milligan CJ, Batten TFC, et al. Neuronal P2X₇ Receptors Are Targeted to Presynaptic Terminals in the Central and Peripheral Nervous Systems. The Journal of Neuroscience. 2001;21(18):7143.
52. Young CNJ, Brutkowski W, Lien C-F, Arkle S, Lochmüller H, Zabłocki K, et al. P2X7 purinoceptor alterations in dystrophic mdx mouse muscles: relationship to pathology and potential target for treatment. Journal of Cellular and Molecular Medicine. 2012;16(5):1026-37.

Acknowledgements – DJ is grateful for the help and supervision of TVG, KL, MS and EP during the experimental work. EW and TVM are thanked for the opportunity to conduct this study under their supervision. TVG, KL and MS are gratefully acknowledged for performing the animal injections. The Cardio and Organ Systems and Neuroimmunology research groups are thanked for providing equipment and reagents.

Author contributions –EW and TVM conceived and designed the research. DJ and TVG performed experiments and data analysis. MS and KL provided assistance with injecting animals. DJ wrote the paper. All authors carefully edited the manuscript.

SUPPLEMENTARY MATERIAL

Supplementary Table 1 – **Primers used for gene expression analysis**

Gene	Forward primer sequence	Reverse primer sequence
CD90	5'-GCTCTCCTGCTCTCAGTCTT-3'	5'-CAGGCGAAGGTTTTGGTTCA-3'
c-Jun	5'GACCTTCTACGACGATGCCC-3'	5'-GCCAGGTTCAAGGTCATGCT-3'
SOX2	5'-GATCAGCATGTACCTCCCCG-3'	5'-CTTAAGCCTCGGGCTCCAAA-3'
SOX10	5'-CACGCAGAAAGCTAGCCGAC-3'	5'-CACTTTCGTTCAGCAACCTCCA-3'
Oct-6	5'-CTCCTGGGGTCCTTCTAACT-3'	5'-TTATACACAGATGCGGCTCTC-3'
p75	5'-CCCTGCCTGGACAGTGTTAC-3'	5'-ACAGGGAGCGGACATACTCT-3'
NCAM	5'-GCCTGAAACCTGAGACGAGG-3'	5'-CTTGGGTGCACTGGGTTCC-3'
Krox-20	5'-GATCACAGGCAGGAGAGACTGC-3'	5'-TCCGTTCATCTGGTCAAAGGG-3'
MPZ	5'-TCTCAGGTCACGCTCTATGTC-3'	5'-GCCAGCAGTACCGAATCAG-3'
MBP	5'-CAGCCAGCACCACTCTTGAA-3'	5'-GCCTCTCCTCGGTGAATCTC-3'

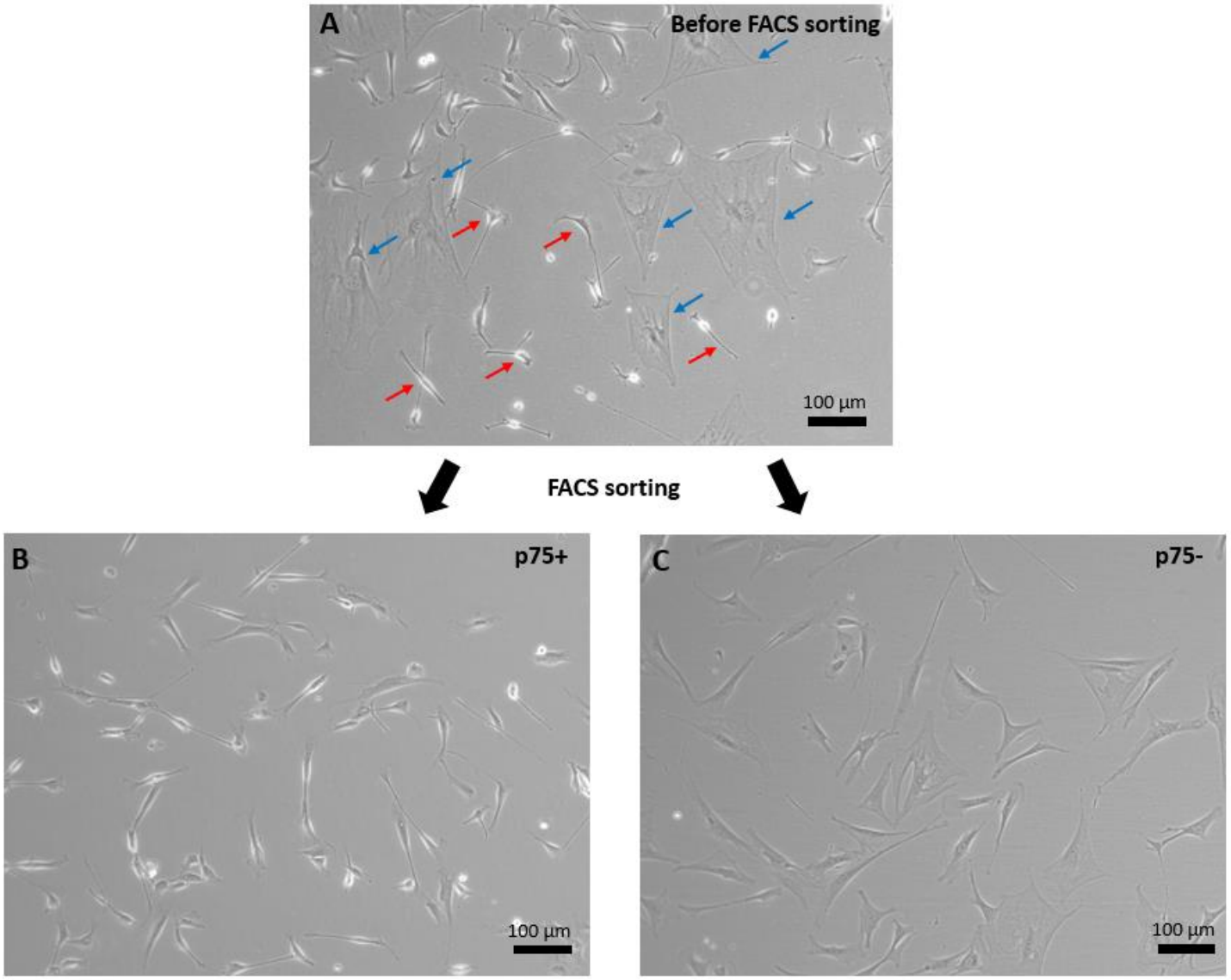

Supplementary Fig. 1 – Primary mouse cells before and after p75 FACS sorting. Phase-contrast images of primary cells isolated from mouse nerve tissue. **(A)** Unsorted cells. Red arrows indicate Schwann cells, spindle-shaped cells with a small cell body and long, thin processes. Blue arrows indicate fibroblasts, flattened cells with a large cell body. **(B)** p75 positive cells after FACS sorting. This culture consists almost solely of cells with a Schwann cell-like morphology. **(C)** p75 negative cells after FACS sorting. This culture consists almost solely of cells with a fibroblast-like morphology.

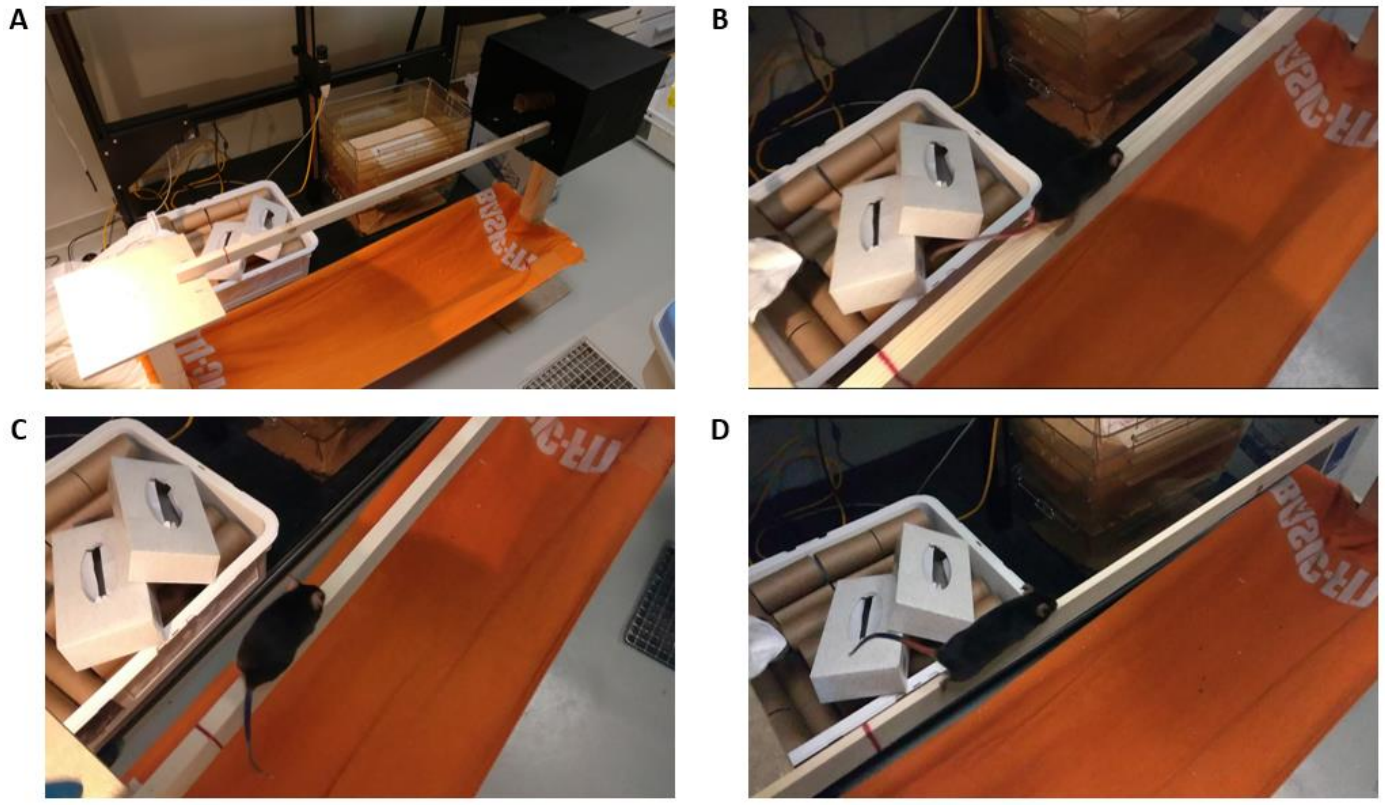

Supplementary Fig. 2 – Beam walk test setup. Mice traversed the beam and the time taken to traverse the inner 80 cm was recorded. **(A)** Photo of the setup. The beam was suspended ~1m above the ground with a black end goal box. Underneath the beam, a towel was suspended to break the animals' fall. **(B)** Mouse traversing the 18 mm beam. **(C)** Mouse traversing the 12 mm beam. **(D)** Mouse traversing the 7 mm beam.

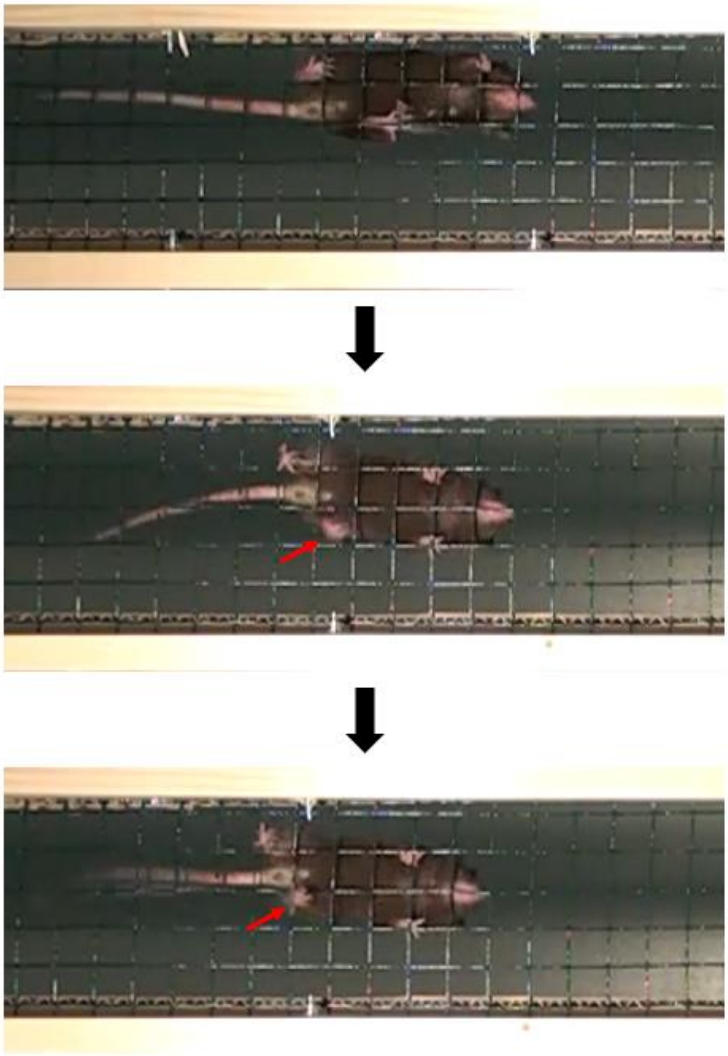

Supplementary Fig. 3 – Example of grid walk assay foot slip. Animals traversed a wire grid and the number of foot slips was recorded. Foot slips were defined as the animal attempting to place a hind paw and completely passing through the plane of the wire grid. Red arrows indicate a hind paw slipping.

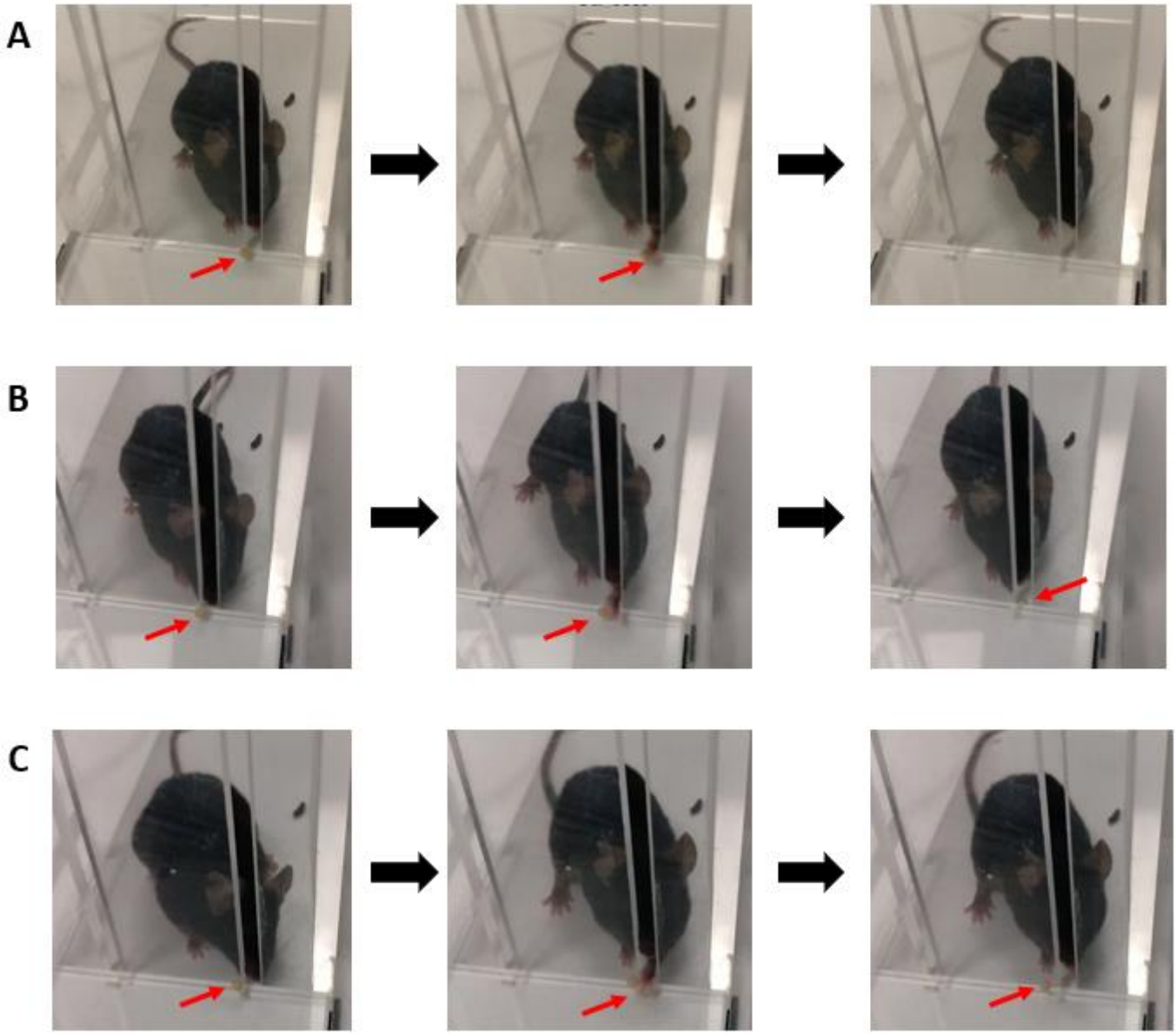

Supplementary Fig. 4 – Scoring used in the pellet retrieval task. Mice were placed in a plastic container and grabbed food pellets from behind a slit in the container wall. Red arrows indicate the food pellet. **(A)** Success. The animal successfully grabs the pellet and feeds it into its mouth. **(B)** Drop. The animal grabs the pellet but drops it before feeding it into its mouth. **(C)** Fail. The animal fails to grab the pellet.

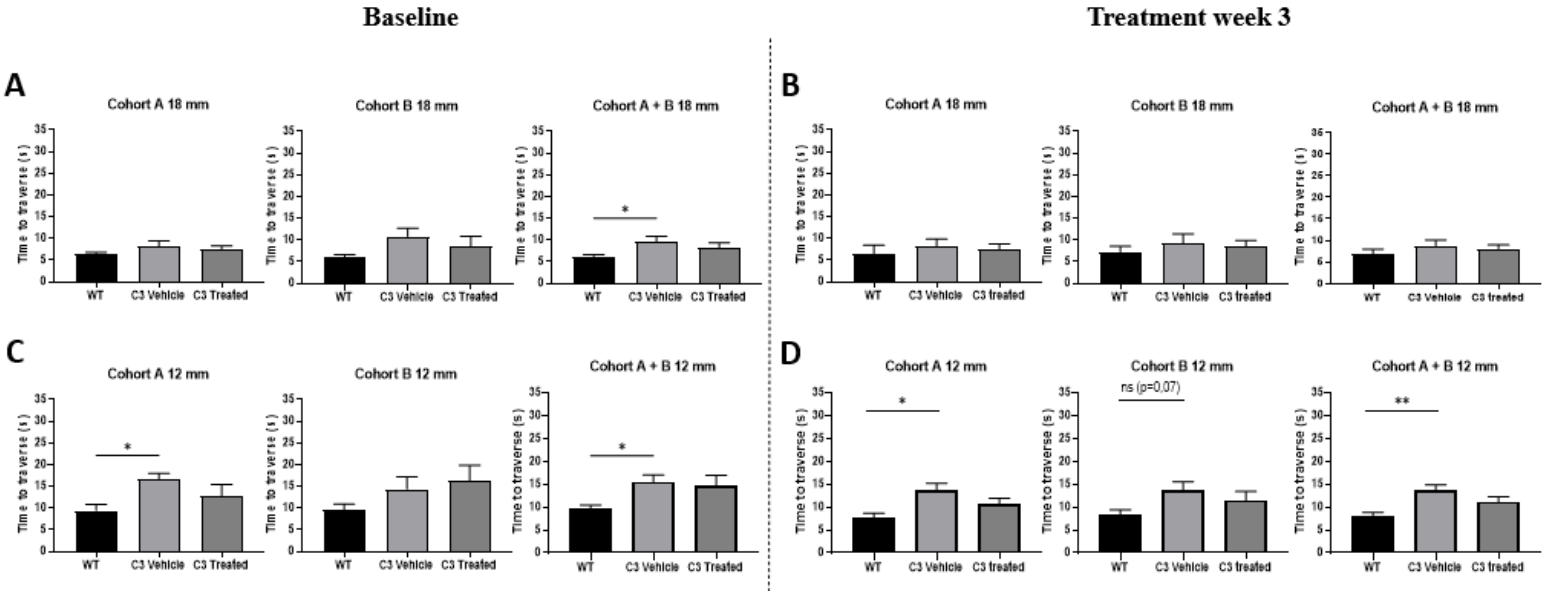

Supplementary Fig. 5 – Beam walk assay using 18 and 12 mm beams. (A, B) 18 mm beam. **(A)** Baseline measurements. Only in the pooled cohorts does the untreated C3 group perform significantly worse than the WT group, while the treated C3 group does not. **(B)** Measurements during week 3 of treatment. There are no significant differences between all 3 groups across all 3 cohorts. **(C, D)** 12 mm beam. **(C)** Baseline measurements. In cohort A and the pooled cohorts, the untreated C3 groups perform significantly worse than the WT group, while the treated C3 group does not. In cohort B, there is no difference between the 3 groups. **(D)** Measurements during week 3 of treatment. In cohort A and the pooled cohorts, the untreated C3 groups perform significantly worse than the WT group, while the treated C3 group does not. In cohort B, there is no difference between the 3 groups. WT, wild type; C3 Vehicle, C3-PMP22 administered DMSO; C3 Treated, C3-PMP22 administered 0,3 mg/kg GEBR-32a. Data are presented as mean ± SEM. Statistical analysis: Kruskal-Wallis test, Dunn multiple comparisons test. *$p \leq 0.05$, **$p \leq 0.01$, ***$p \leq 0.001$.